

26. MAJOR ELEMENT, TRACE ELEMENT, AND ISOTOPE (Pb, Sr, AND Nd) VARIATIONS IN SITE 834 BASALTS: IMPLICATIONS FOR THE INITIATION OF BACKARC OPENING¹

Janet M. Hergt² and Kristen Nilsson Farley³

ABSTRACT

New major, trace element, and isotope data (Pb, Sr, and Nd) reveal an impressive compositional variation in the basalts recovered from Site 834. Major element compositions span almost the entire range observed in basalts from the modern axial systems of the Lau Basin, and variations are consistent with low-pressure fractionation of a mid-ocean-ridge-basalt (MORB)-like parent, in which plagioclase crystallization has been somewhat suppressed. Trace element compositions deviate from MORB in all but one unit (Unit 7) and show enrichments in large-ion-lithophile elements (LILEs) relative to high-field-strength elements (HFSEs) more typically associated with island-arc magmas. The Pb-isotope ratios define linear trends that extend from the field of Pacific MORB to highly radiogenic values similar to those observed in rocks from the northernmost islands of the Tofua Arc. The Sr-isotope compositions also show significant variation, and these too project from radiogenic values back into the field for Pacific MORB.

The variations in key trace element and isotopic features are consistent with magma mixing between two relatively mafic melts: one represented by Pacific MORB, and the other by a magma similar to those erupted on 'Eua when it was part of the original Tongan arc, or perhaps members of the Lau Volcanic Group (LVG). Based on our model, the most radiogenic compositions (Units 2 and 8) represent approximately 50:50 mixtures of these MORB and arc end-members.

Magma mixing requires that both components are simultaneously available, and implies that melts have not shown a compositional progression from arc-like to MORB-like with extension at this locality. Rather, it is apparent that essentially pristine MORB can erupt as one of the earliest products of backarc initiation. Indeed, repetition of isotopic and trace element signatures with depth suggests that eruptions have been triggered by periodic injections of fresh MORB melts into the source regions of these magmas. The slow and almost amagmatic extension of the original arc complex envisaged to explain the observed chemistry is also consistent with the horst-and-graben topography of the western side of the Lau Basin.

Given the similarities between basalts erupted at the modern Lau Basin spreading centers and MORB from the Indian Ocean, the overwhelming evidence for involvement of mantle similar to Pacific MORB in the petrogenesis of basalts from Site 834 is a new and important observation. It indicates that the original arc was underlain by asthenospheric material derived from the Pacific mantle convection cell, and that this has somehow been replaced by Indian Ocean MORB during the last ~5.5 Ma.

INTRODUCTION

True seafloor spreading, as observed in the Lau Basin today (Parson et al., 1990), is a relatively recent phenomenon and was not in operation during the initial stages of basin evolution (Lawver and Hawkins, 1978; Parson et al., 1992; Parson and Hawkins, this volume). By characterizing the earliest available products of backarc magmatism in the Lau Basin (those from Leg 135, Site 834), we seek to investigate the initiation mechanism of backarc rifting as well as the magmatic consequences of the transition from arc to backarc volcanism.

One consequence of backarc basin formation has been to produce both a remnant arc (i.e., the Lau Ridge) and a modern arc (i.e., the Tofua Arc), but how and where the initial rifting occurs is the subject of much debate. Not wishing to argue for or against any particular model, we will use the terms "arc-rupture" and "arc-rifting" to signify either splitting and separation within the arc (e.g., Karig, 1970) or rifting of the arc-forearc complex in general (Hawkins et al., 1984).

The geochemical consequences of backarc basin evolution on magmatism have been the subject of much speculation (e.g., Tarney et al., 1981; Hawkins and Melchior, 1985), and identification of any progressive change in magma type with basin evolution was a major objective of the Leg 135 drilling program. Based on dredging of rare

exposed rocks in the older portions of backarc basins and the similarities of backarc basin basalts to normal MORB (N-MORB) at well-developed spreading centers, it had been suggested that backarc basin magmas progressively evolve from "arc-like" to "MORB-like" in their geochemical characteristics (Hawkins and Melchior, 1985). Such a progressive geochemical evolution would produce a compositionally zoned basin floor, reflecting the continuous migration of the source of the arc volcanics away from the site of the mantle upwelling producing the backarc basin volcanics. This is of particular interest because although supporting evidence comes from the Mariana Trough (e.g., Stern et al., 1990), a recent study of the volcanics accompanying the incipient rifting behind the Izu-Bonin Arc (Sumisu Rift) concluded that the volcanics are chemically distinct from the nearby arc and do not support models of a progressive change in magma composition (Fryer et al., 1990).

Causes for the initiation of backarc opening remain a subject of discussion. Taylor and Karner (1983) noted that if backarc opening was simply linked to convection in the wedge (induced by subduction of the downgoing plate), then all arcs should have associated backarcs, and this is not the case. Although remaining controversial, growing consensus exists that backarc opening is related to changes in the profile of the downgoing slab, although it is not always clear whether this is a cause or an effect of the change in stress regime. Changes in the slab profile may result from readjustment of the relative motions of the converging plates (e.g., Furlong et al., 1982; Hynes and Mott, 1985; Jarrard, 1986), and in many models, it is envisaged that a change in the slab dip is a key feature; some of the parameters that have been investigated include the age of the subducting crust, the convergence rate, and absolute plate motion.

In addition, and possibly more importantly, slab rollback is becoming increasingly favored as the mechanism by which tension is

¹ Hawkins, J., Parson, L., Allan, J., et al., 1994, *Proc. ODP, Sci. Results*, 135: College Station, TX (Ocean Drilling Program).

² Department of Earth Sciences, the Open University, Walton Hall, Milton Keynes, MK7 6AA, United Kingdom (present address: School of Earth Sciences, The University of Melbourne, Parkville, Victoria, 3052, Australia).

³ Scripps Institution of Oceanography, University of California, San Diego, La Jolla, CA 92093, U.S.A. (present address: Department of Geology, Whittier College, Whittier, CA 90608, U.S.A.).

introduced into the overriding plate (e.g., Garfunkel et al., 1986). In this case, the change in slab profile is the result of rollback, and rollback itself is the cause of trench migration and tension within the arc.

The specific way in which backarc initiation takes place will control the magmatic products erupted. Some processes might permit a progressive change away from arc magmatism and toward compositions similar to MORB. It is also possible that gradual chemical evolution is not required, and that even in the earliest stages, magmatism might reflect the composition of the underlying mantle in the region (i.e., unaffected by the arc).

Considering the tectonic regime of the Lau Basin in particular, backarc opening occurred simultaneously with the clockwise rotation of the Tonga Trench and the modern Tofua Arc relative to the Lau Ridge (Fig. 1). Rotation has been greatest in the north, where the subduction rate is highest (Hynes and Mott, 1985), so that backarc extension has propagated from north to south. Hergt and Hawkesworth (this volume) speculate on the way in which slab rollback may have controlled the clockwise rotation of the trench drawing on supporting evidence provided from published subduction rates and changes in the slab dip toward the north.

GEOGRAPHIC SETTING

The location of Site 834 is at approximately 18°34'S, 177°52'W and is described in detail in the Initial Reports volume (Parson, Hawkins, Allan, et al., 1992). Site 834 is the closest of the Leg 135 sites to the Lau Ridge, the presently inactive predecessor to the Tofua Arc, and therefore is also the most likely of the Leg 135 sites to have seen the influence of the sub-arc mantle source (Fig. 1).

It was originally thought that backarc opening first began in the Lau Basin at approximately 3 Ma (Karig, 1970) or <5 Ma (Gill, 1976), by which time much of the magmatism had ceased at the abandoned Lau Ridge. The age of sediments overlying the basement material at Site 834 provide a minimum estimate for the time of basin opening: 5.6 Ma. This older age, together with the age data for samples from the Lau Ridge (Gill, 1976) suggests that basalts were being emplaced in the backarc while volcanism in the Lau Islands was still active. Contemporaneous arc and backarc magmatism during the initial stages of extension is particularly significant when trying to identify the processes operative during backarc opening.

SAMPLE SELECTION AND ANALYTICAL TECHNIQUES

Site 834 was drilled twice. Hole A extends to a depth of 149.50 mbsf and 5 igneous units between 106.2 mbsf and the bottom of the hole were intersected; Hole B was drilled to a depth of 435.30 mbsf. The recovery of basaltic material appears to depend on the nature of the flows with large massive units being more successfully recovered compared with thin or pillowed flows. A more detailed account of the extent of drilling and recovery at Site 834 is described in the relevant section of the *Initial Reports* volume for Leg 135 (Parson, Hawkins, Allan, et al., 1992); however, overall recovery for Hole 834B was approximately 30%. The shipboard study of basement samples recovered at Site 834 during Leg 135 identified 13 petrographic units; representative samples from most of these units were selected for analysis here. Most of the samples analyzed are from glass rinds carefully chipped from pillow margins.

Major element compositions of the natural glasses were analyzed on the Cameca SX-50 electron microprobe at the University of California, Davis. Each reported major element analysis represents an average of at least five analyses; spot size was generally 15 μm . The operating current was 15 Kv and sample current was 10 na. Natural mineral standards were used and basalt glass JDFD2 was employed to monitor drift and the data were normalized where necessary (see Nilsson, this volume). Mineral analyses were performed under similar

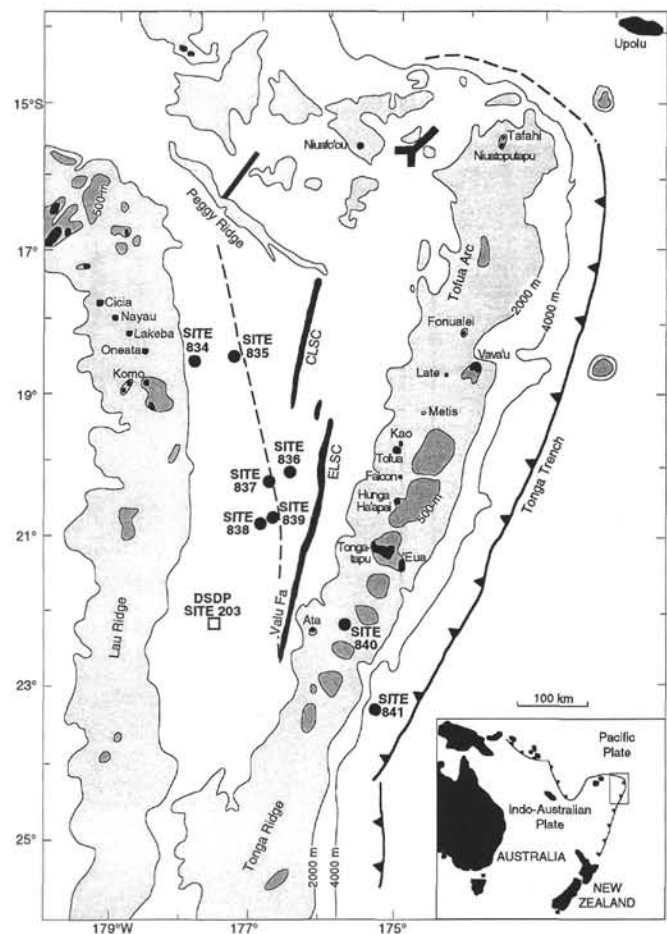


Figure 1. General geography of the Lau Basin area indicating the location of Site 834 in relation to the Lau Ridge, the Tonga Ridge, and the "Central" and "Eastern" Lau Spreading Centers (CLSC and ELSC, respectively; collectively termed "modern Lau" or "ML" in this study). The dashed line extending from the Peggy Ridge to the Valu Fa Ridge approximates the division between horst-and-graben topography (in the west) from new crust formed by true seafloor spreading (to the east). The position of this line is based on the work of Parson and Hawkins (this volume) and also represents the locus of the southward-propagating ELSC ridge tip. Light and dark shading is used to represent regions between 2000–500 mbsf and 500–0 mbsf, respectively. The darkest gray is used to indicate neovolcanic zones (e.g., ELSC and CLSC); except for the drill sites, black depicts land.

conditions except that the spot size used was 1–3 μm for clinopyroxene and oxides, and 7–10 μm for plagioclase.

Trace element concentrations were obtained using the inductively coupled plasma mass spectrometer (ICP-MS) at Durham University. The data represent whole-rock concentrations as it was considered desirable to take representative samples for analysis, rather than attempt to bias the samples toward "glass only" compositions by removing phenocrysts.

Sample digestion (without prior leaching) was conducted in the clean Pb-isotopic laboratory at the Open University. Because acid leaching is likely to result in element loss from the glass, the ICP-MS samples were cleaned using a rapid ultrasonic wash in acetone (to remove any grease derived from the drilling and the red-wax pencil used to mark the sample request on board the ship). The chips were then rinsed three times in pure "Millipore" reverse osmosis water in an ultrasonic bath, and dried in air. Further "crushing" was achieved by "cracking" the chips using a clean agate mortar and pestle. No

grinding was attempted so as to eliminate the contamination derived from the crushing apparatus. Digestion and analysis were conducted as described in Hergt and Sims (this volume).

The samples chosen for isotopic analyses are the same as those analyzed by ICP-MS, and these were prepared and handpicked in the same manner as that described above. As it is the isotopic compositions of Pb, Sr, and Nd that are critical in these analyses, and not the absolute abundances of these elements, the samples were leached before dissolution, first in 1M HBr, and then in ~3M HCl to remove contamination from seawater and sample handling (see Hergt and Hawkesworth, this volume, for further details). Certain tests were run to examine the effectiveness of the leaching stages and ability of removing any possible seawater alteration. These are described in more detail in Hergt and Hawkesworth (this volume) and suggest that the range of values observed in samples from Site 834 is geologically relevant and not the result of alteration processes.

The data presented in Tables 1–3 consist of representative plagioclase, clinopyroxene, and oxide analyses respectively. Table 4 includes the major element analyses for all glass samples, whereas Table 5 lists the trace element and isotopic results obtained on the 25 samples chosen for more detailed analysis. Three of the samples from Table 5 lack major element data, as these are aphyric samples rather than glass, and could not be measured using the electron microprobe.

RESULTS

Mineralogy and Petrography

Full details of the petrographic characteristics of these samples are presented in the site report in the Leg 135 Initial Reports volume (Parson, Hawkins, Allan, et al., 1992). They range from aphyric basalts (Units 1, 2, 4, 6, and 8 and Subunit 10a) to plagioclase-phyric basalts (Units 3 and 7) to plagioclase-olivine-phyric basalts (Units 9 and 11) to olivine-clinopyroxene-plagioclase-phyric basalts (Units 12 and 13). Unit 5 is a diabasic sill comprised of large poikilitic clinopyroxene crystals enclosing small plagioclase laths. Phenocryst abundances are generally quite low (<5%), and only Unit 7 is densely phyric (>15% phenocrysts). Unit 12 is unique in containing Fe-Ti oxide phenocrysts in the glassy rim, suggesting that this was a liquidus phase at the time of eruption. Although no other unit contains oxide phenocrysts, skeletal oxides occur in the interstitial mesostasis of most other units and are relatively large in the coarse-grained Unit 5.

Representative phenocryst compositions were obtained from Subunits 2a and 10a and Units 5, 7, and 12. Plagioclase (Units 5, 7, and 12), clinopyroxene compositions (Unit 5), and Fe-Ti oxide compositions (all units) are presented in Tables 1–3, respectively. Additional data, including olivine and Cr-spinel analyses, are presented in Hawkins and Allan (this volume). Ewart et al. (this volume) also present graphical compilations of the plagioclase, olivine and pyroxene compositions for the units from Site 834. Based on our own

results, plagioclase phenocrysts exhibit a large range in composition (An_{23} – An_{85}) with most between An_{55} and An_{65} . None are extensively zoned and An variations within a grain are rarely greater than 10%. There are, however, very narrow, presumably sodic, rims on many of the large plagioclase grains. Although we do not have compositional data on these rims, they may be produced during devolatilization associated with eruption and the subsequent stabilization of more sodic compositions. Unit 5, the diabase with poikilitic texture, is unique in that it exhibits a large range in plagioclase compositions. Small laths of plagioclase enclosed in the pyroxenes in Unit 5 have relatively high and consistent compositions (An_{55} – An_{70}), whereas the large interstitial grains exhibit a much greater compositional range and extend to significantly more sodic compositions (An_{24} – An_{72}). The more protected laths enclosed in clinopyroxene megacrysts may have been isolated from late-stage changes in magma composition and subsolidus re-equilibration events. Plagioclase compositions in Unit 7 (An_{60} – An_{76}) are somewhat more calcic than those in Unit 12 (An_{53} – An_{58}), consistent with the more evolved liquid compositions of Unit 12.

Compositions of the large poikilitic clinopyroxene megacrysts in Unit 5 are relatively homogeneous ($Wo_{39-45}En_{33-47}$), and chemical zonation within a grain was rarely observed. Both ilmenite (ilmenite-hematite solid solutions) and titanomagnetite (magnetite-ulvöspinel solid solutions) were observed and analyzed in the relatively coarse-grained Unit 5. Most units contain small interstitial titanomagnetite crystals (Table 3). Unit 12 is the only other unit with abundant oxides: euhedral titanomagnetite grains (Usp_{40-45}) in the glassy rim and small phenocrysts in the interior. Petrographic evidence for subsolidus re-equilibration of titanomagnetite (e.g., development of oxyexsolution lamellae) is rare and such grains were avoided during microprobe analysis.

Vesicle content is generally high and variable in the Site 834 lavas. Excluding Unit 7, the whole-rock interiors contain from 10 to 45 vol% vesicles as large as 5 mm in size. Unit 7 is unique among these samples and is essentially nonvesicular. Indeed, Unit 7 is the only nonvesicular unit recovered from any of the backarc sites on Leg 135.

As noted in the site report (Parson, Hawkins, Allan, et al., 1992), most of the samples are relatively fresh, secondary mineralization is minimal, and most vesicles are devoid of infilling. Flow morphologies differed in the various units from relatively massive flows or sills (Unit 5) to pillow fragments with abundant glassy margins (Subunits 2a and 10a and Units 6, 7, 8, 11, 12, and 13).

Major Element Geochemistry

Because glass margins represent chilled liquids and sufficient glass was recovered at Site 834, we will concentrate on inferences made from glass compositions in the following discussion. Except in the case of K_2O , shipboard X-ray fluorescence (XRF) spectrometry data (Parson, Hawkins, Allen, et al., 1992) generally follow the same

Table 1. Representative plagioclase compositions obtained for Units 5, 7, and 12.

Unit	5 c	5 r	5 c	5 r	5 c	5 r	5 l	5 l	5 l	7 l	7 l	7 l	7 l	7 c	7 r	7 c	7 r	12 l	12 l	12 l
Na ₂ O	7.72	8.55	5.12	4.14	3.05	3.59	5.06	3.47	4.52	3.79	4.38	3.69	4.45	3.93	4.45	2.65	3.47	4.67	4.83	5.03
Al ₂ O ₃	25.16	23.33	28.97	29.90	31.77	31.06	28.56	30.85	29.90	30.06	28.44	30.32	29.66	30.35	29.08	32.48	31.00	29.28	29.39	27.80
SiO ₂	60.67	63.72	55.29	52.72	50.61	51.22	55.11	51.53	53.62	52.70	53.29	52.70	53.71	52.99	53.69	49.51	51.76	52.52	54.78	54.97
K ₂ O	0.11	0.13	0.02	0.06	0.04	0.06	0.03	0.06	0.08	0.01	0.04	0.01	0.00	0.04	0.05	0.03	0.03	0.01	0.04	0.05
CaO	6.64	4.83	10.93	12.31	14.72	13.96	11.40	14.06	12.30	13.19	11.98	13.56	12.45	13.32	12.30	15.36	14.14	11.53	11.79	10.65
FeO	0.53	0.37	0.65	0.85	0.62	0.77	0.52	0.57	0.70	0.73	1.30	0.45	0.52	0.67	0.72	0.33	0.35	0.71	0.91	1.20
Total	100.83	100.91	100.98	99.97	100.80	100.66	100.68	100.54	101.12	100.49	99.43	100.72	100.79	101.31	100.29	100.35	100.75	98.72	101.74	99.71
Ab	67.4	75.7	45.8	37.7	27.2	31.7	44.5	30.8	39.7	34.2	39.7	33.0	39.3	34.7	39.5	23.7	30.6	42.2	42.5	45.9
Or	0.6	0.7	0.1	0.3	0.2	0.3	0.2	0.4	0.5	0.1	0.2	0.1	0.0	0.2	0.3	0.2	0.2	0.1	0.2	0.3
An	32.0	23.6	54.1	62.0	72.6	68.0	55.3	68.9	59.8	65.7	60.0	66.9	60.7	65.0	60.3	76.1	69.2	57.7	57.3	53.8

Notes: Unit 5: adjacent "c" and "r" are cores and rims of large grains, respectively; "l" = small laths enclosed within poikilitic clinopyroxene grains. Unit 7: "l" = lath-shaped microlites; adjacent "c" and "r" are cores and rims of equant phenocrysts, respectively. Unit 12: all analyses are of small microlites in the glassy rim.

Table 2. Representative clinopyroxene compositions obtained for Unit 5.

Unit	5	5	5	5	5	5	5	5	5	5
Na ₂ O	0.41	0.40	0.26	0.36	0.35	0.29	0.20	0.27	0.44	0.35
MgO	10.60	11.25	14.59	14.71	14.77	14.46	16.87	16.26	13.32	14.54
Al ₂ O ₃	2.65	2.87	3.23	3.42	3.41	1.58	1.78	3.57	3.15	3.78
SiO ₂	48.73	48.91	51.83	51.64	51.38	53.07	54.19	52.74	49.92	51.03
CaO	18.93	19.57	21.01	21.24	21.21	18.82	20.93	22.14	19.69	19.88
TiO ₂	1.80	1.53	1.09	1.20	1.10	0.92	0.55	0.73	1.70	1.28
MnO	0.43	0.32	0.19	0.28	0.18	0.27	0.20	0.17	0.30	0.28
FeO*	16.41	14.28	8.50	8.29	8.41	11.25	6.65	5.42	11.88	9.79
Total	99.97	99.13	100.72	101.13	100.83	100.67	101.37	101.33	100.40	100.92
Wo	41.9	43.2	43.7	44.5	44.8	39.3	42.1	45.5	42.6	42.1
En	32.6	34.6	42.2	42.9	43.4	42.0	47.2	46.5	40.1	42.8
Fs	25.5	22.2	14.1	12.6	11.9	18.8	10.7	8.1	17.3	15.1

Table 3. Representative oxide compositions obtained for Subunits 2a and 10a and Units 5, 7, and 12.

Unit or subunit	2a	5	5	7	10a	10a	12	12	12
SiO ₂	0.09	0.08	0.16	0.14	0.10	0.11	0.07	0.11	0.09
TiO ₂	18.15	20.03	19.70	23.61	15.56	15.61	14.95	14.80	14.63
Al ₂ O ₃	1.67	0.38	2.56	1.33	2.70	3.08	3.78	3.80	3.76
Fe ₂ O ₃	32.19	29.54	27.72	21.73	36.43	35.35	37.35	37.66	37.90
MgO	0.94	0.69	1.40	0.62	2.27	2.37	3.68	3.73	3.70
MnO	0.79	0.73	0.60	0.74	0.50	0.48	0.36	0.34	0.49
FeO	46.05	47.93	47.32	51.80	41.94	42.43	40.04	40.04	39.65
CaO	0.03	0.07	0.06	0.13	0.06	0.07	0.11	0.04	0.03
Total	99.89	99.45	99.51	100.11	99.56	99.49	100.33	100.53	100.24
x [*]	0.54	0.57	0.61	0.70	0.46	0.48	0.45	0.44	0.44

Notes: All analyses are of small, euhedral grains with no evidence for oxyexsolution or alteration. Only data from Unit 12 are from phenocrysts in the glassy rim; the other data are from interstitial grains.

trends defined by the glass data, suggesting that most of the whole rocks are not significantly modified from liquid compositions. The K₂O contents are somewhat higher in the whole rocks than the glasses (0.2%–0.7% vs. 0.1%–0.3%, respectively) and may reflect some growth of K-rich alteration phases in the crystalline interiors. For the most part, the units distinguished on the basis of their macroscopic characteristics on board the ship also define chemically homogeneous units (Table 4). The only petrographic units showing significant within-unit chemical heterogeneities were Unit 6 and Subunit 10a. Unit 6 was divided into Subunits 6a, 6b, and 6c, and the single anomalous composition in Subunit 10a is identified as 10a*. It should also be noted that the lowermost sample from Unit 12 and the uppermost one from Unit 13 were apparently mislabeled (presumably during shipboard sampling); these have been transposed in Table 4.

A wide variety of major element characteristics occur in the basalts from Site 834 (Fig. 2). For comparison, Figure 2 also includes fields representing N-MORB and lavas from the actively spreading Eastern and Central Lau Spreading Centers (ELSC and CLSC, respectively). It has been established in numerous studies that basalts produced in backarc basins deviate somewhat from N-MORB compositions, particularly with respect to TiO₂, FeO*, and Al₂O₃ contents (e.g., Hawkins and Melchior, 1985; Sinton and Fryer, 1987; Hawkins et al., 1990; Fryer et al., 1990). The Site 834 rocks are no exception and are similar (in some respects) to many modern backarc basin basalts. Although it is desirable to compare the compositions of basalts from Site 834 with those from other backarc sites drilled during Leg 135, this would add considerable clutter to Figure 2. Instead we simply note overlap between some of the Site 834 compositions (and trends) with those from Sites 835 and 836, and significant apparent differences between samples from Sites 837, 839 and perhaps 838 (for detailed comparisons, refer to the introductory section of the *Initial Results* volume for Leg 135; Parson, Hawkins, Allan, et al., 1992).

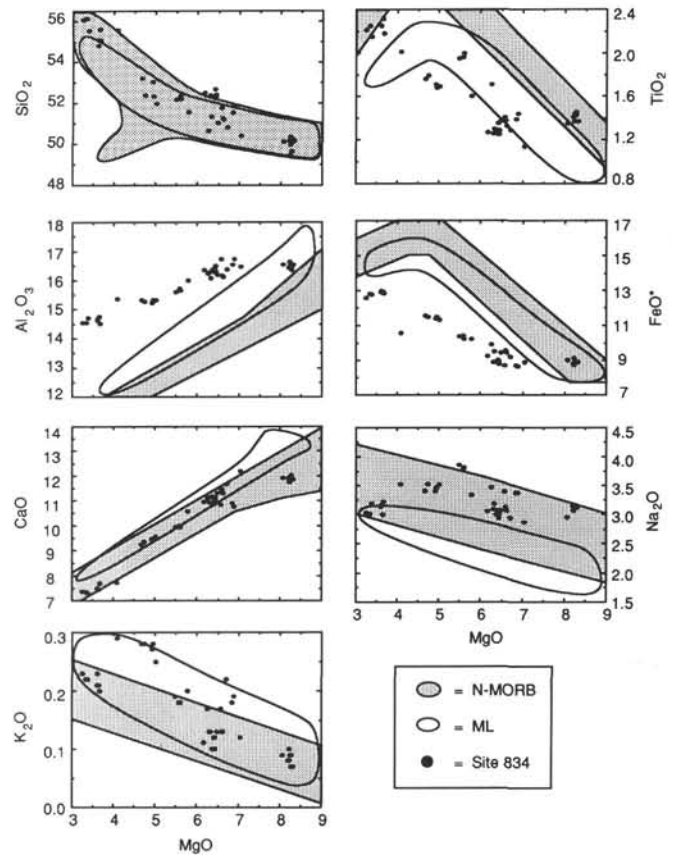


Figure 2. Major element compositions (in wt%) samples from Site 834. The stippled field represents the range for MORB compiled by Hochstaedter et al. (1990), which includes data from Byerly et al. (1976), Byers et al. (1983), Schilling et al. (1983), Bender et al. (1984), le Roex et al. (1985), and Christie and Sinton (1986). Bold lines enclose fields for data from the modern spreading centers in the Lau Basin (ELSC and CLSC). Data sources are Ernewein et al. (in press), Hawkins and Allan (this volume), and Hawkins (unpubl. data). For a comparison between samples from Site 834 and the other sites drilled during Leg 135, the reader is referred to the introductory chapter of Parson, Hawkins, Allan, et al. (1992). ML = modern Lau Basin.

The range in major element geochemical compositions for the samples from this single site is nearly as great as that observed in the entire axial system of the Lau Basin today (Fig. 2). Major element chemistries range from low SiO₂–high MgO basalts identical to N-MORB (Unit 7), to basaltic andesites with nearly 56 wt% SiO₂ (Unit 12). When comparing fractionation trends in Figure 2, trends for SiO₂, CaO, and K₂O essentially overlap both the N-MORB and ML fields.

The fractionated Site 834 lavas (Subunits 10a and 10a* and Unit 12) clearly follow the SiO₂ enrichment trend of MORB. TiO₂, FeO*, Al₂O₃, and Na₂O of the Site 834 lavas all deviate from both the N-MORB and ML trends. Despite their increase with fractionation, TiO₂ and FeO* have shallower slopes than either N-MORB or ML. Although liquidus titanomagnetite is observed in the Unit 12 samples, no obvious decrease is evident in either TiO₂ or FeO* among the most fractionated units, suggesting that extensive fractionation of Fe-Ti oxides has not occurred. Compared with both N-MORB and ML data, Al₂O₃ in the Site 834 glasses is 2–3 wt% higher at a given MgO content, and the slope with decreasing MgO is somewhat shallower. Na₂O contents are relatively high in these glasses and no obvious fractionation trend is apparent.

The composition of Unit 7 is distinct from the rest of the Site 834 lavas in many respects. For several elements, the Unit 7 composition

Table 4. Major element compositions for Site 834 glasses.

Core, section, interval (cm)	Unit or subunit	SiO ₂	TiO ₂	Al ₂ O ₃	FeO	MnO	MgO	CaO	Na ₂ O	K ₂ O	P ₂ O ₅	Total
135-834A-												
13X-1, 18-24	2a	50.62	1.71	16.24	9.90	0.16	6.27	11.12	3.47	0.17	0.24	99.90
14X-1, 25-31	2a	51.57	1.60	16.01	10.20	0.18	5.78	10.57	3.33	0.20	0.20	99.64
135-834B-												
14R-1, 28-32	6a	52.34	1.96	15.71	10.42	0.18	5.59	9.99	3.77	0.18	0.25	100.39
15R-1, 0-8	6b	50.79	1.29	16.38	9.19	0.17	6.72	11.66	2.93	0.22	0.21	99.56
15R-2, 35-37	6a	52.20	2.00	15.64	10.21	0.16	5.61	9.94	3.81	0.18	0.28	100.03
15R-2, 96-104	6a	52.16	1.95	15.59	10.36	0.18	5.50	9.94	3.85	0.19	0.25	99.97
18R-1, 0-6	6c	51.55	1.39	16.55	8.70	0.13	6.86	10.91	3.37	0.18	0.20	99.84
18R-1, 7-13	6c	51.83	1.44	16.73	8.65	0.12	6.90	10.77	3.37	0.19	0.20	100.20
19R-1, 5-10	6c	51.76	1.41	16.74	8.68	0.18	6.58	10.85	3.39	0.17	0.20	99.96
22R-1, 41-46	7	50.12	1.37	16.53	8.87	0.17	8.32	11.76	3.12	0.07	0.15	100.49
26R-1, 107-109	7	49.97	1.44	16.53	8.95	0.16	8.26	11.92	3.14	0.09	0.16	100.62
30R-2, 98-104	7	50.09	1.35	16.53	9.01	0.18	8.08	11.91	2.95	0.09	0.14	100.34
31R-1, 98-104	7	50.23	1.43	16.46	8.87	0.16	8.28	12.03	3.16	0.09	0.16	100.87
31R-2, 37-42	7	49.62	1.45	16.35	8.94	0.16	8.28	12.00	3.12	0.07	0.15	100.14
31R-2, 43-48	7	50.12	1.41	16.42	8.82	0.17	8.21	11.91	3.15	0.08	0.16	100.44
32R-1, 0-5	7	49.44	1.37	16.64	9.10	0.16	8.23	11.83	3.14	0.08	0.15	100.16
33R-1, 0-6	7	50.32	1.43	16.44	8.71	0.17	8.22	11.75	3.06	0.10	0.18	100.39
34R-2, 60-63	8	52.49	1.27	16.36	9.24	0.16	6.16	10.96	3.05	0.11	0.14	99.94
35R-1, 15-23	8	52.66	1.35	16.28	8.85	0.15	6.43	10.88	3.01	0.10	0.13	99.84
35R-1, 31-37	8	52.36	1.26	16.29	8.88	0.15	6.30	10.93	3.09	0.13	0.13	99.52
35R-2, 67-69	8	52.23	1.25	16.41	8.99	0.19	6.42	11.10	3.06	0.12	0.10	99.86
35R-2, 70-72	8	52.35	1.29	16.31	8.94	0.13	6.45	11.13	2.98	0.10	0.09	99.77
35R-2, 77-83	8	52.36	1.28	16.31	8.89	0.18	6.45	11.01	2.93	0.10	0.11	99.63
36R-1, 0-7	8	52.40	1.25	16.50	8.76	0.12	6.44	10.99	3.00	0.12	0.11	99.70
36R-1, 7-10	8	52.32	1.28	16.38	8.92	0.16	6.37	11.16	2.99	0.12	0.11	99.80
37R-2, 42-44	10a*	55.57	2.01	15.36	10.56	0.16	4.09	7.72	3.52	0.29	0.32	99.61
39R-1, 0-7	10a	51.97	1.69	15.32	11.33	0.18	5.02	9.56	3.51	0.25	0.21	99.04
39R-1, 7-10	10a	53.04	1.71	15.23	11.38	0.19	4.92	9.45	3.41	0.27	0.20	99.80
39R-1, 9-15	10a	52.33	1.68	15.31	11.49	0.21	4.94	9.48	3.46	0.28	0.23	99.40
40R-1, 45-47	10a	52.37	1.79	15.28	11.47	0.19	4.74	9.32	3.52	0.28	0.21	99.16
41R-1, 0-5	10a	53.21	1.76	15.31	11.55	0.21	4.67	9.22	3.41	0.28	0.24	99.86
46R-1, 37-40	11	50.39	1.14	16.48	8.89	0.15	7.06	12.20	2.86	0.12	0.15	99.45
47R-1, 130-135	12	55.54	2.15	14.70	12.75	0.25	3.38	7.29	3.18	0.22	0.31	99.77
50R-1, 87-92	12	56.06	2.21	14.54	12.56	0.27	3.24	7.35	3.03	0.23	0.28	99.77
51R-1, 10-15	12	56.15	2.25	14.55	12.79	0.28	3.34	7.32	3.01	0.22	0.28	100.19
53R-1, 7-20	12	55.08	2.18	14.52	12.84	0.25	3.69	7.68	3.22	0.20	0.29	99.95
54R-1, 0-5	12	55.59	2.31	14.75	12.92	0.24	3.65	7.43	2.99	0.21	0.28	100.37
54R-1, 5-10	12	55.10	2.25	14.69	12.97	0.25	3.62	7.49	3.16	0.23	0.27	100.03
57R-1, 0-5	12	54.80	2.25	14.62	12.87	0.25	3.60	7.47	3.14	0.21	0.28	99.50
56R-2, 111-118	13	51.26	1.38	16.16	9.56	0.17	6.59	11.44	3.12	0.13	0.14	99.94
57R-1, 34-40	13	51.20	1.33	16.11	9.44	0.16	6.62	11.32	3.06	0.13	0.13	99.49
59R-2, 30-32	13	51.34	1.30	16.07	9.52	0.16	6.33	11.14	3.18	0.13	0.17	99.35
59R-2, 52-55	13	51.02	1.38	16.18	9.45	0.15	6.49	11.32	3.06	0.13	0.15	99.34

*Single anomalous composition in Subunit 10a.

is much more similar to N-MORB at comparable MgO than any of the other units. The MORB-like character is particularly clear for TiO₂ and FeO* concentrations. For both CaO and Al₂O₃, Unit 7 is displaced from the general fractionation trend; this displacement is well into the MORB field in the case of CaO and obviously toward it in the case of Al₂O₃.

Trace Element Geochemistry

With the exception of Unit 7, significant departures from N-MORB trace element compositions occur in the basalts from Site 834 (Table 5). Almost all of the samples analyzed show marked enrichments in Cs, Rb, Ba, K, Pb, and Sr and a depletion in Nb (relative to U) compared with N-MORB (Figs. 3A-3B). The smooth trace element pattern exhibited by Unit 7 samples further illustrates their similarity to N-MORB. Although Units 2, 5, 7, 8, 11, and 13 have approximately N-MORB abundances of the more compatible elements (P to Yb on Fig. 3C), Units 6 and 12 and Subunit 10a have abundances of almost twice N-MORB for these elements. In addition, Units 2, 6, 10, and 12 show greater enrichment in the elements Cs to Pb (Fig. 3B) compared with Units 5, 8, 11, and 13 (Fig. 3A).

Some aspects of these trace element characteristics are similar to island-arc basalts (IABs). Enrichment in LILEs (e.g., Cs, Rb, Ba, K), depletion in Nb relative to U, and enrichment in Pb relative to Ce are shared by IAB and continental rocks. In many of the Site 834 samples, ratios such as Ce/Pb and Nb/U show significant deviations from the values expected in oceanic basalts: Ce/Pb = ~25 and Nb/U = ~50

(Hofmann et al., 1986). The Ce/Pb ratio varies from about 13 (Unit 8) to 27 (Unit 7), whereas the Nb/U ratio varies from approximately 10 (Units 2 and 10) to 47 (Unit 7). The low values approach those observed in rocks from either the continental crust or arcs (Ce/Pb = ~4 and Nb/U = ~10).

Interestingly, those elements showing enrichments above N-MORB concentrations correlate reasonably well with each other, but not necessarily with other major and trace element concentrations. For example, Ba and Rb are elements with comparable and highly incompatible behavior during the crystallization of olivine, pyroxene ± plagioclase and therefore should (1) increase with decreasing MgO, (2) correlate with each other, and (3) maintain a uniform Ba/Rb ratio. Although the Ba contents of the Site 834 basalts correlate well with Rb and MgO, the Ba/Rb ratio varies independently of MgO (Fig. 4). Similar diagrams can be generated for the other "enriched" elements; these diagrams demonstrate that, although fractional crystallization may serve to increase the abundances of the incompatible elements as expected, some additional process has also influenced the concentrations of these elements. Several other incompatible elements appear to have very poor correlations with MgO content (e.g., Fig. 5); however, these elements may actually generate two subparallel trends with respect to MgO as suggested by the dashed lines on the plot of Nb vs. MgO.

Compared with the ML volcanics, some samples from Site 834 have significantly higher Ba/Rb and lower absolute Nb contents (Sunkel, 1990; Ernewein et al., in press). For example, despite their similar La contents, La/Nb of the Site 834 volcanics is approximately

Table 5. Trace element and isotopic data for selected representative samples from Site 834.

Core, section, interval (cm)	Unit or subunit	Rb	Sr	Y	Zr	Nb	Cs	Ba	La	Ce	Pr	Nd	Sm	Eu	Gd	Tb	Dy	Ho	Er
135-834B-																			
8R-2, 10-913	2	1.14	235	32.7	109.0	1.60	0.02	34.7	3.48	12.20	1.71	9.37	3.12	1.14	4.01	0.80	4.57	0.97	2.98
11R-3, 83-86	5	1.46	207	26.0	86.1	1.10	0.02	25.7	2.67	8.58	1.37	7.56	2.39	0.96	3.25	0.59	3.87	0.82	2.31
13R-1, 130-131	5	1.22	184	23.6	75.4	0.97	0.03	27.4	2.60	8.18	1.32	7.77	2.67	1.03	3.45	0.61	3.71	0.80	2.30
14R-1, 28-32	6	1.45	188	44.5	163.0	2.08	0.04	25.7	4.63	15.21	2.53	14.05	4.77	1.64	6.05	1.12	6.63	1.43	4.34
15R-2, 35-37	6	1.49	193	44.9	165.2	2.15	0.03	26.4	5.00	15.12	2.47	14.12	4.48	1.65	6.13	1.10	6.77	1.46	4.46
15R-2, 96-104	6	1.64	186	43.6	163.3	2.17	0.04	24.7	4.84	14.94	2.50	14.18	4.65	1.68	6.43	1.21	6.67	1.42	4.36
18R-1, 7-13	6	1.89	165	33.6	115.2	1.66	0.03	23.1	4.22	12.57	2.11	11.69	3.85	1.46	5.06	0.95	5.66	1.22	3.73
26R-1, 107-109	7	0.64	175	29.2	104.1	1.41	0.01	5.3	3.36	10.88	1.77	9.95	3.24	1.25	4.38	0.85	5.02	1.10	3.10
31R-1, 98-104	7	1.15	189	29.3	104.2	1.51	0.04	7.1	3.54	11.03	1.69	10.01	3.22	1.24	4.32	0.77	4.79	1.00	3.03
31R-2, 43-48	7	0.64	187	29.4	105.3	1.57	0.03	5.8	3.37	10.68	1.73	9.86	3.34	1.34	4.35	0.78	4.93	1.02	3.02
33R-1, 0-6	7	0.34	185	30.2	106.6	1.59	0.01	4.5	3.43	10.95	1.72	10.33	3.49	1.31	4.52	0.82	5.15	1.07	3.18
33R-2, 105-110	7	0.44	178	24.4	78.0	1.28	0.01	3.0	2.91	9.10	1.48	8.24	2.81	1.06	3.71	0.65	3.84	0.86	2.57
34R-2, 60-63	8	0.98	169	26.2	77.9	0.97	0.04	35.5	2.21	7.59	1.27	7.87	2.76	1.04	3.89	0.67	4.29	0.94	2.66
35R-1, 15-23	8	1.18	176	27.6	79.6	0.96	0.04	35.6	2.24	7.48	1.26	7.77	2.90	1.03	3.84	0.71	4.48	0.98	2.78
35R-2, 77-83	8	1.19	180	27.9	82.5	0.90	0.05	35.1	2.36	7.64	1.29	7.53	2.84	1.01	3.71	0.74	4.33	0.92	2.70
36R-1, 0-7	8	1.11	176	27.7	80.7	0.89	0.04	34.4	2.18	7.54	1.22	7.67	2.84	1.04	3.83	0.68	4.32	0.99	2.64
37R-2, 42-44	10a	3.97	176	61.8	198.2	1.82	0.09	51.7	5.49	17.64	2.93	17.67	5.92	2.03	7.98	1.55	9.37	2.08	6.23
39R-1, 9-15	10a	3.53	213	37.2	114.1	1.16	0.06	47.1	3.69	11.08	1.80	10.32	3.50	1.30	4.82	0.89	5.44	1.21	3.53
40R-1, 45-47	10a	3.42	209	38.3	117.6	1.19	0.10	49.5	3.78	11.52	1.81	10.88	3.69	1.28	4.94	0.97	5.72	1.26	3.71
46R-1, 37-40	11	1.52	168	24.6	70.1	0.78	0.04	29.5	2.45	7.65	1.29	7.91	2.57	1.08	3.58	0.52	3.83	0.83	2.51
47R-1, 130-135	12	2.03	201	47.8	160.0	1.58	0.05	50.2	4.65	14.68	2.46	14.76	4.95	1.67	6.90	1.00	7.37	1.59	4.70
49R-1, 142-144	12	0.74	213	48.0	160.2	1.65	0.01	36.0	4.40	14.35	2.37	13.43	4.46	1.66	6.41	1.11	7.22	1.63	4.52
53R-1, 9-15	12	2.32	196	45.4	156.2	1.61	0.10	49.7	4.34	14.87	2.57	14.06	4.77	1.78	6.63	0.98	7.76	1.59	4.69
56R-2, 111-118	13	1.48	177	28.4	82.4	0.95	0.05	29.3	2.60	8.52	1.40	8.45	2.91	1.10	4.07	0.60	4.58	0.95	2.82
59R-2, 52-55	13	1.46	169	27.3	79.0	0.95	0.05	29.4	2.44	8.28	1.34	8.42	2.86	1.23	4.01	0.62	4.45	0.91	2.77

Core, section, interval (cm)	Unit or subunit	Tm	Yb	Lu	Hf	Ta	W	Ti	Pb	Th	U	²⁰⁶ Pb/ ²⁰⁴ Pb	²⁰⁷ Pb/ ²⁰⁴ Pb	²⁰⁸ Pb/ ²⁰⁴ Pb	⁸⁷ Sr/ ⁸⁶ Sr	¹⁴³ Nd/ ¹⁴⁴ Nd
135-834B-																
8R-2, 10-913	2	0.46	2.63	0.44	2.31	0.12	0.06	0.06	0.92	0.17	0.11	18.781	15.554	38.428	0.702841	0.513111
11R-3, 83-86	5	0.38	2.14	0.38	1.99	0.16	0.03	0.04	0.59	0.12	0.06	18.738	15.529	38.324	0.702782	0.513121
13R-1, 130-131	5	0.35	1.97	0.42	1.70	0.09	0.03	0.16	1.31	0.10	0.05	18.730	15.528	38.333		
14R-1, 28-32	6	0.61	3.73	0.78	3.49	0.20	0.04	0.08	0.72	0.18	0.07	18.643	15.509	38.177	0.702626	
15R-2, 35-37	6	0.64	3.96	0.81	3.45	0.16	0.01	0.05	0.78	0.16	0.09	18.617	15.480	38.093	0.702674	0.513122
15R-2, 96-104	6	0.65	3.83	0.83	3.49	0.18	0.02	0.08	4.42	0.15	0.07	18.638	15.500	38.147	0.702618	0.513125
18R-1, 7-13	6	0.53	3.13	0.71	2.75	0.13	0.04	0.07	1.07	0.19	0.07	18.584	15.505	38.095	0.702637	0.513123
26R-1, 107-109	7	0.46	2.65	0.58	2.28	0.10	0.04	0.08	0.64	0.07	0.03	18.561	15.482	38.027	0.702524	
31R-1, 98-104	7	0.40	2.59	0.55	2.27	0.10	0.02	0.09	0.46	0.07	0.04	18.572	15.476	38.026	0.702542	0.513109
31R-2, 43-48	7	0.42	2.55	0.55	2.26	0.10	0.01	0.04	0.44	0.09	0.04	18.593	15.502	38.035		0.513122
33R-1, 0-6	7	0.47	2.73	0.61	2.32	0.11	0.02	0.06	0.41	0.08	0.04	18.572	15.467	38.028		0.513113
33R-2, 105-110	7	0.37	2.10	0.43	1.75	0.12	0.02	0.04	0.50	0.07	0.06	18.605	15.494	38.081	0.702544	
34R-2, 60-63	8	0.40	2.42	0.55	1.77	0.06	0.02	0.05	0.56	0.05	0.04	18.767	15.527	38.384	0.702774	
35R-1, 15-23	8	0.40	2.34	0.57	1.84	0.08	0.02	0.05	0.57	0.06	0.03	18.769	15.534	38.398	0.702746	
35R-2, 77-83	8	0.42	2.45	0.59	1.80	0.06	0.03	0.02	0.57	0.07	0.03	18.790	15.546	38.425	0.702776	0.513119
36R-1, 0-7	8	0.39	2.31	0.51	1.93	0.07	0.02	0.07	0.53	0.08	0.04	18.776	15.534	38.395	0.702958	
37R-2, 42-44	10a	0.86	5.44	1.39	4.70	0.49	0.03	0.08	1.23	0.28	0.13	18.677	15.534	38.395	0.702780	0.513117
39R-1, 9-15	10a	0.52	3.18	0.79	2.56	0.23	0.04	0.07	0.90	0.23	0.12	18.722	15.523	38.297		0.513121
40R-1, 45-47	10a	0.56	3.31	0.89	2.77	0.12	0.05	0.07	0.87	0.23	0.11	18.732	15.533	38.328	0.702914	0.513111
46R-1, 37-40	11	0.36	2.16	0.45	1.71	0.09	0.04	0.04	0.60	0.13	0.05	18.680	15.514	38.245	0.702808	0.513109
47R-1, 130-135	12	0.72	4.14	0.80	3.93	0.18	0.06	0.05	0.99	0.14	0.09	18.731	15.516	38.293	0.702868	
49R-1, 142-144	12	0.75	3.95	0.69	3.75	0.13	0.04	0.03	0.97	0.14	0.51	18.712	15.495	38.243	0.702896	0.513113
53R-1, 9-15	12	0.66	4.48	0.77	3.98	0.17	0.04	0.05	0.99	0.13	0.11	18.738	15.525	38.320	0.702891	0.513110
56R-2, 111-118	13	0.47	2.43	0.44	2.15	0.09	0.05	0.05	0.58	0.11	0.05	18.701	15.518	38.275	0.702802	0.513116
59R-2, 52-55	13	0.38	2.59	0.38	2.14	0.34	0.08	0.07	0.58	0.08	0.05	18.700	15.512	38.270	0.702811	

2.5, whereas that of the ML is 1.5 (Ernewein et al., in press). In addition, ML volcanics tend to have depletions in Sr relative to Nd, whereas the Site 834 samples exhibit Sr enrichment. Because all samples from the ML show high Rb and Ba compared with Zr, Ti, and the heavy rare earth elements (HREEs), none of the ML lavas exhibit the smooth trace element patterns displayed by Unit 7. The MORB-like magmas of Unit 7 (≥ 5.6 Ma) are therefore closer to true N-MORB compositions than anything presently erupting at the modern Lau Basin spreading centers.

Isotope Geochemistry

Sr and Nd Isotopes

The position of rocks from Site 834 in Sr- vs. Nd-isotopic space relative to other fields for rocks in the geographic vicinity is illustrated in Figure 6. The Sr-isotopic compositions from Site 834 show vari-

ations well in excess of analytical uncertainty, and range from 0.70252 to 0.70291. The lowest ⁸⁷Sr/⁸⁶Sr ratios occur in the rocks from Unit 7. Importantly, these compositions lie within the field for Pacific MORB and represent the lowest ⁸⁷Sr/⁸⁶Sr thus far reported for rocks from the Lau Basin (see also Hergt and Hawkesworth, this volume). Although the range is significant, the highest values do not reach the values more typical of the ML spreading centers (~0.7033; e.g., Volpe et al., 1988; Loock et al., 1990; J.M. Hergt, unpubl. data, 1989).

In contrast with Sr, the Nd-isotopic compositions of Site 834 samples are very uniform (0.51312 ± 0.00003 , 2σ variation) and are similar to both MORB and those rocks from the ML with the highest ¹⁴³Nd/¹⁴⁴Nd ratios. The constant Nd-isotopic signature of samples from Sites 834 produces a field that extends from Pacific MORB toward the low Sr-high Nd end of the modern Lau Basin array. The data field from Site 834 does not project down toward the field for samples from the Tofua Arc.

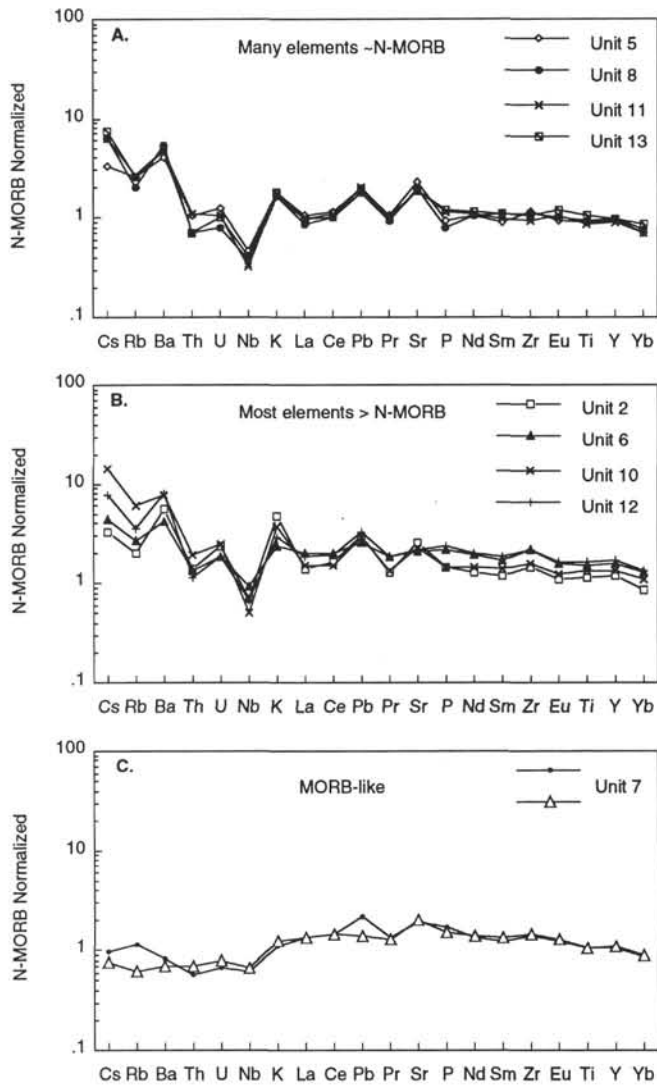


Figure 3. N-MORB normalized trace element compositions of representative samples from each unit recovered at Site 834. Normalizing values used are those for the N-MORB listed in Sun and McDonough (1989). Although similar in shape, subtle differences in the degree of enrichment is evident between units shown in Figures 3A and 3B (see text). Contrasting with all other units is the smooth, more MORB-like pattern of Unit 7 (Fig. 3C).

Pb Isotopes

The Pb-isotope compositions of basalts from Site 834 define linear trends in Pb-isotope space (Fig. 7). Compared with the modern arc and backarc compositions, the least radiogenic samples from Site 834 share similar $^{208}\text{Pb}/^{204}\text{Pb}$ and $^{207}\text{Pb}/^{204}\text{Pb}$ values but at much higher $^{206}\text{Pb}/^{204}\text{Pb}$. Unlike ML basalts, the Site 834 trends extend from within the Pacific MORB field (rather than in the field for Indian Ocean MORB) up to radiogenic values similar to the island compositions from 'Ata and 'Eua, toward the field for Tafahi and Niuatoputapu.

In detail, systematic changes in the Pb-isotopic ratios occur with depth (Fig. 8). Samples from the top of the core (Unit 2) have among the most radiogenic compositions, and a progressive decrease in the Pb-isotopic ratios occurs with depth producing minimum values in the samples from Unit 7. The Pb-isotope ratios increase sharply below this level with Unit 8 rocks showing values similar to those of Unit 2. Again, the compositions become less radiogenic with depth. Thus, a progressive variation is present in the Pb-isotope ratios downhole,

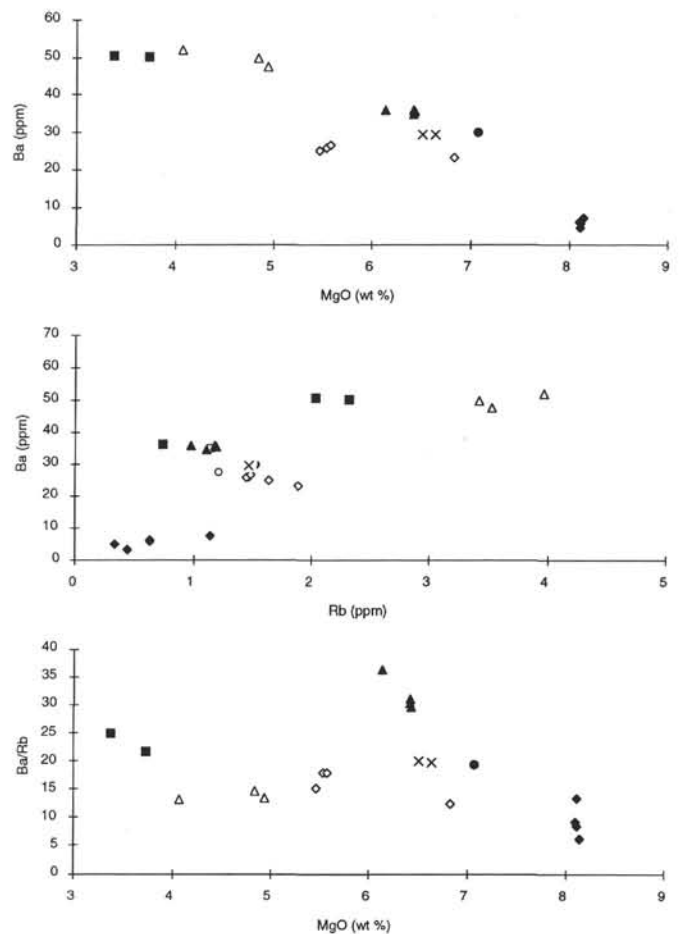


Figure 4. Variations among Ba, Rb, and MgO. Note the strong correlations between Ba and MgO and for Ba vs. Rb as well as the absence of any covariation between the Ba/Rb ratio and MgO content. Symbols represent individual unit designations and are as follows: Unit 2 (open square), Unit 5 (open circle), Unit 6 (open diamond), Unit 7 (filled diamond), Unit 8 (filled triangle), Unit 10 (open triangle), Unit 11 (filled circle), Unit 12 (filled square), and Unit 13 (crosses).

which might point to some form of cyclic behavior in the petrogenesis of the Site 834 basalts. Figure 8 shows that similar variations are also observed in the Sr-isotope ratios.

DISCUSSION

The linearity of the Pb-isotope variations (and comparable ranges in Sr-isotope ratios) suggest that at least part of the compositional variability observed at Site 834 may result from two-component mixing. This raises several fundamental questions concerning the petrogenesis of the Site 834 lavas, including (1) What is the cause of the major element variations? Do these variations also reflect mixing? (2) What end-members were involved? Do these components resemble any other volcanics observed in the region? (3) When did mixing occur relative to melt generation and fractional crystallization? and (4) How do the mixing processes help to identify the processes that occurred during the initiation of backarc rifting in the Tonga-Lau Basin system?

Fractional Crystallization and Major Element Variations

The trends produced by the Site 834 data (Fig. 2) are broadly consistent with fractionation of olivine, plagioclase, and clinopyrox-

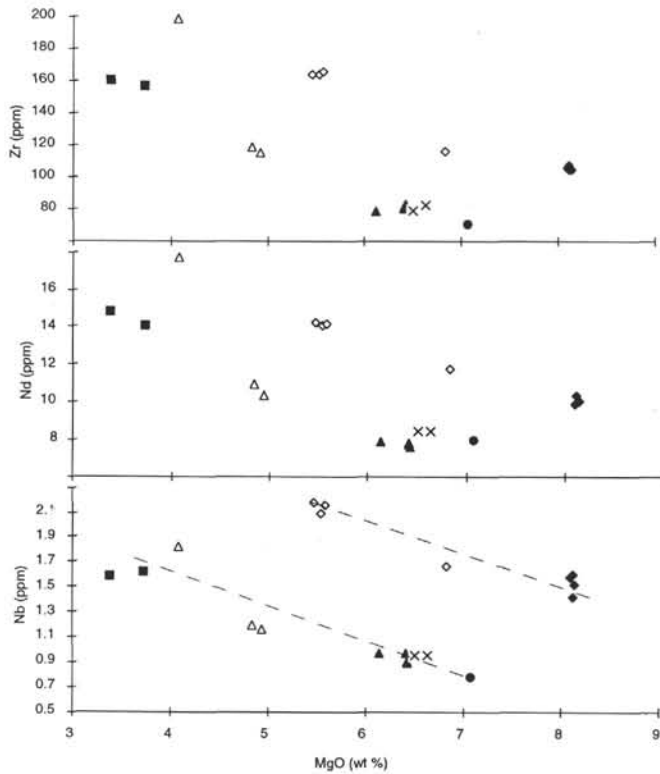


Figure 5. Apparently scattered variations between HFSEs and REEs with MgO, which may actually represent subparallel evolutionary trends (as suggested by the use of dashed lines in the plot of Nb vs. MgO). Symbols as in Figure 4.

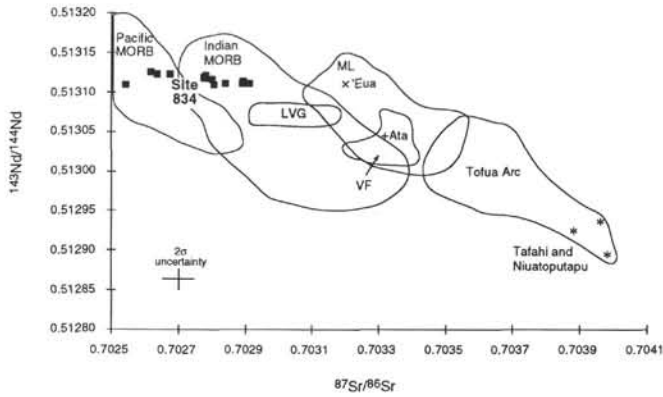


Figure 6. Sr- vs. Nd-isotopic ratios for Site 834 samples shown relative to fields for Pacific and Indian MORB, volcanics from the Lau Ridge (LVG; Cole et al., 1990), Tofua Arc ('Ata, Tafahi, and Niuaotupapu indicated; data from Ewart and Hawkesworth [1987] and J.M. Hergt, unpubl. data, 1989), and samples from the modern Lau Basin spreading centers (Volpe et al., 1988; Look et al., 1990; J.M. Hergt, unpubl. data, 1989). The forearc island of 'Eua is also shown (McCulloch, unpubl. data, from Cole et al., 1990). Symbols as in Figure 4. ML = modern Lau Basin.

ene; that is, SiO₂, TiO₂, FeO*, and K₂O increase with decreasing MgO, whereas Al₂O₃ and CaO decrease as MgO decreases. Although the general fractionation processes may be similar, there are significant differences between the trends of these data and N-MORB. In particular, we will address the relatively high Al₂O₃ and low FeO* and TiO₂ contents, and the relative uniformity of most major element abundances in the compositional range 6–9 wt% MgO.

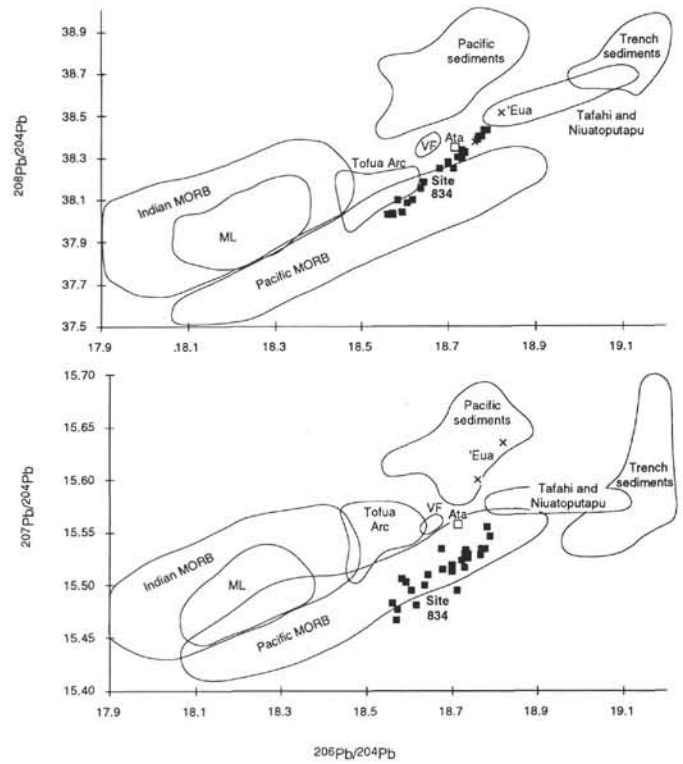


Figure 7. Pb-isotope compositions of the samples from this study (filled squares), shown in reference to fields for Pacific and Indian MORB, Pacific, and trench sediments (Ben Othman et al., 1989; J.M. Hergt, unpubl. data, 1989); modern Lau Basin (Look et al., 1990; J.M. Hergt, unpubl. data, 1989); the Valu Fa Ridge (Jenner et al., 1987); and Tongan islands (Oversby and Ewart, 1972; Ewart and Hawkesworth, 1987; J.M. Hergt, unpubl. data, 1989).

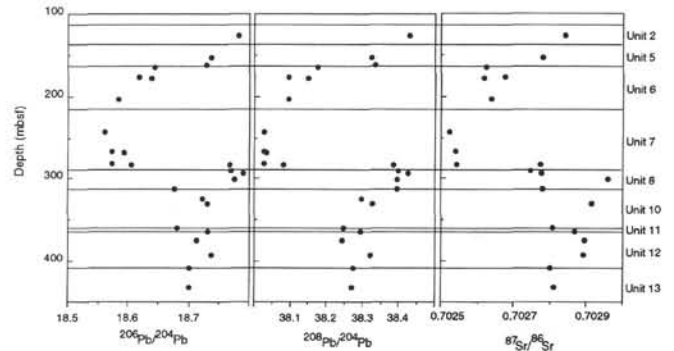


Figure 8. Pb- and Sr-isotope data from Site 834 shown vs. depth in meters below seafloor (mbsf). The horizontal lines mark the boundaries between units, and unit designations are given on the right-hand side of the diagram. Note the extreme ratios of Units 2, 7, and 8, the sharp increase in ratios from Unit 7 to Unit 8, and the more gradual change in ratios with depth elsewhere.

We have modeled the fractionation trends by calculating the liquid line of descent (LLD) from various selected starting compositions. Although a number of programs are available for use in calculating LLDs in anhydrous systems (e.g., Nielsen, 1988; Weaver and Langmuir, 1990), there are none that incorporate the effects of water saturation or undersaturation. In addition to the widely held hypothesis that backarc lavas are generated in a water-present system, the Site 834 lavas exhibit elevated oxygen fugacity and alkali element concentrations that are postulated to result from interaction with a fluid phase

(Nilsson, this volume). The predominant effect of water on the LLD of a basaltic composition is to delay the arrival of plagioclase on the ol-cpx-pl cotectic. Suppression of plagioclase is intuitively appealing for the Site 834 data because it is consistent with the absence of a decrease in Al_2O_3 during the early stages of crystallization.

Although the quantitative effects of water on LLD calculations have not been determined, the qualitative effects have recently been discussed by Langmuir et al. (in press). In order to calculate the LLD for a suite of arc lavas, Langmuir et al. (in press) have modified the LLD program of Weaver and Langmuir (1990) such that it simulates plagioclase suppression by lowering the plagioclase-liquid distribution coefficients (K_d) for the An and Ab components in accord with experimental data (Drake, 1976; Helz, 1976; Spulber and Rutherford, 1983). It is important to note that elevated water contents may also effect the mineral-liquid K_d s of olivine and clinopyroxene, and that it is difficult to calibrate the K_d s that we have used with the actual H_2O contents in the melt. For these reasons, the calculated LLDs shown on Figure 9 should be taken as a qualitative illustration of the effects of water undersaturation on the crystallization of these lavas. Further experimental data on hydrous systems are crucial before arc and backarc LLDs can be qualitatively modeled.

We have calculated LLDs for various starting compositions at a range of possible water contents and crystallization pressures. Although we have been unable to model the Site 834 data precisely, our most successful attempt is illustrated in Figure 9. The hypothetical starting composition used was chosen to be similar to Unit 7 (and therefore also similar to relatively primitive MORB), pressure was 1 kilobar (kb) and plagioclase crystallization was effectively delayed until MgO concentration reached 7 wt% by olivine and clinopyroxene fractionation (bold lines). The anhydrous LLD for the same starting composition and pressure is shown for comparison (dashed line). In the anhydrous situation, plagioclase reaches the liquidus at approximately 8.5 wt% MgO. A delay in plagioclase saturation has a profound effect on the FeO, TiO_2 , and Al_2O_3 fractionation trends, whereas the effect on SiO_2 , CaO, and Na_2O is relatively minor. The calculated LLDs are extremely well matched to the data in the cases of FeO* and Al_2O_3 , moderately well matched in the cases of SiO_2 and CaO, and only matched for some of the data in the cases of TiO_2 and Na_2O . With respect to most elements, the general shape of the LLD compares well with the trend defined by the data. In particular, the flat patterns for many elements between 6 and 9 wt% MgO are reproduced extremely well.

Although the LLD in CaO-MgO space predicts compositions somewhat higher than are observed in this data set, we are encouraged by the similar shape of the LLD and the trend of the data. We have experimented with different starting compositions, yet this LLD is particularly robust and all starting compositions ultimately follow this trend. Successful attempts were made to improve the fit to the TiO_2 and Na_2O data by modifying the starting compositions. Because TiO_2 and Na_2O contents are very sensitive to melting processes and source differences, our inability to model all of the variations in those elements from a single starting composition suggests that these variations may reflect the fractionation of different parental compositions. We note, for example, the close match between values calculated for these components using the starting composition shown in Figure 9, and the data from Subunits 2a and Units 6 and 7.

The LLD program that we used only predicts the effects of plagioclase, olivine, and clinopyroxene crystallization. In order to estimate the effects of Fe-Ti oxide crystallization on these lavas we have made least-squares calculations using the program MULTIFIT provided by Bryan (1986). Except for Subunit 10a and Unit 12, variable amounts of plagioclase, olivine, and clinopyroxene fractionation can, in fact, explain most of the variation observed. The FeO* and TiO_2 data do not suggest the removal of large amounts of Fe-Ti oxides; however, to generate compositions similar to Subunit 10a and Unit 12, approximately 2%–3% titanomagnetite must be removed from any reasonable parent.

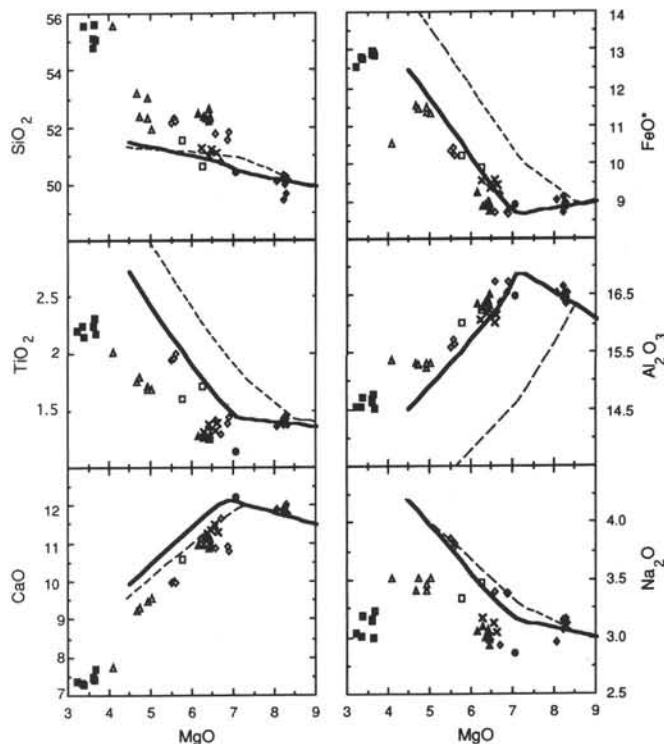


Figure 9. Site 834 glass data and calculated liquid lines of descent as described in the text; symbols as in Figure 4. The heavy solid line represents the "wet" LLD at 1 kb, and the dashed line shows the LLD for the anhydrous case. A hypothetical MORB-like starting composition was used.

We conclude, therefore, that the major element variations in the Site 834 glasses are consistent with fractionation of a MORB-like starting composition in a hydrous system at approximately 1 kb pressure. Although not entirely successful, our modeling provides excellent agreement with the data for FeO* and Al_2O_3 , and also reproduces the shapes of the trends for TiO_2 and CaO. We interpret this as strong support for fractionation in a system where plagioclase crystallization is suppressed until approximately 7 wt% MgO, reflecting the presence of water in the system. Scatter in the TiO_2 and Na_2O data suggests the presence of different parental compositions, supporting the interpretation of incompatible trace element and radiogenic isotope data as discussed below.

Although this hypothesis is consistent with most of the glass data, we are left to explain the presence of small plagioclase phenocrysts in Unit 7. Recall that by our model, Unit 7 formed before plagioclase began crystallizing. We speculate that perhaps devolatilization associated with eruption left the melt supersaturated with respect to plagioclase and triggered the crystallization that is observed in the quenched phase assemblage without having a significant influence on the glass composition.

Identification of Mixing Components

Characterization of the end-member mixing components is a fundamental issue in understanding the mantle composition and processes operating beneath the Tonga-Lau Basin system during back-arc opening.

The composition of basalts from Unit 7 suggests that one of the mantle end-members was similar to N-MORB in composition. In addition to MORB-like major element concentrations, the Unit 7 samples have the high Ce/Pb, high Nb/U, and the smooth trace element patterns characteristic of N-MORB (e.g., Fig. 3C). The unradiogenic

Pb- and Sr-isotopic compositions of Unit 7 (Figs. 6–7) are also very similar to MORB compositions. Importantly, the Pb and Sr signatures of Unit 7 are typical of Pacific N-MORB mantle and not the Indian Ocean mantle that is thought to underlie the Lau Basin at the present time (e.g., Hergt and Hawkesworth [this volume], and consistent with the results of Loock et al. [1990] from the ML). Thus, we suggest that one end-member composition is closely matched by Pacific MORB, and, given the close similarity between Unit 7 and N-MORB, we have used the average composition of Unit 7 as the N-MORB end-member in the following calculations.

The other end-member is broadly "arc-like" in composition: low Ce/Pb, low Nb/U, radiogenic Sr- and Pb-isotopic ratios. To constrain this composition further, we have compared it with various volcanics from the modern Tofua Arc and its predecessor, the Lau Ridge. We are somewhat limited by the dearth of combined isotope and trace element data from the various islands, but the Pb signatures of the Site 834 rocks suggest that Pb-isotopic compositions of the "arc" component are highly radiogenic compared with the values characteristic of most of the Tofua Arc. The Pb composition of this component is more similar to the unusual lavas from Tafahi and Niuatoputapu (the northernmost islands of the Tofua Arc). Ewart and Hawkesworth (1987) commented on the similarity between the Pb-isotopic signatures of these younger islands and those from 'Eua, the only representative of the ancient arc from the Tonga Ridge (although they also noted that some dispute exists regarding the exact $^{207}\text{Pb}/^{204}\text{Pb}$ values of at least one of the 'Eua samples). Thus, although most of the Tofua Arc magmatism exhibits less radiogenic Pb compositions, the northernmost islands may preserve the radiogenic signatures of the original Tongan arc as observed at 'Eua (Ewart and Hawkesworth, 1987; see also Hergt and Hawkesworth, this volume).

Similarities in their Pb-isotope compositions suggests that the "arc" component at Site 834 might resemble those from the source tapped at 'Eua (old Tongan arc) or Tafahi (northern Tofua Arc). We will now attempt independently to calculate the trace element composition of this component, and compare our model composition with the signatures of these proposed end-members. To compare elemental compositions, it is desirable to correct for the effects of fractional crystallization that may have modified the original concentrations. Although the extent of fractionation of these samples can be estimated from major element concentrations, mixing has resulted in the preferential enrichment of some elements in some units beyond the effects of fractionation. Fortunately, the most and least radiogenic units (8 and 7, respectively) are among the least fractionated units recovered at Site 834. Although Unit 8 is somewhat more fractionated than Unit 7 ($\text{Mg}\# = 59$ vs. 65 [$\text{Mg}\# = \text{Mg}/\text{Mg} + \text{Fe}^{2+}$; $\text{Fe}_2\text{O}_3/\text{FeO} = 0.15$]), the effect of this on the trace element signatures is minor compared with that of mixing (Fig. 10).

Variations in elements such as Ba and Rb (which are enriched in Unit 8) correlate with each other but are not entirely linked with indices of fractional crystallization (Fig. 4). As these elements have similar incompatibility during partial melting and fractional crystallization, Ba/Rb should not covary with MgO; Figure 4 illustrates that this is indeed the case. The fact that differences in Ba/Rb occur at all requires the operation of an additional process, and the correlation between $^{206}\text{Pb}/^{204}\text{Pb}$ and Ba/Rb shown in Figure 11 provides convincing evidence that Ba/Rb variations are controlled by mixing.

Not all incompatible elements are enriched in Unit 8 relative to Unit 7; some elements (e.g., Nb and P) are actually depleted in Unit 8 relative to Unit 7 (Fig. 10). Because Unit 8 is somewhat more fractionated than Unit 7, the concentrations of these incompatible elements would have increased with fractionation and the original depletions of these elements may have been even more pronounced.

If we make the simplifying assumption that fractional crystallization has not obscured the results of mixing for Units 7 or 8, we can calculate the trace element composition of a model arc component capable of mixing with Unit 7 to generate Unit 8. The results of these simple mass-balance calculations can then be compared with compo-

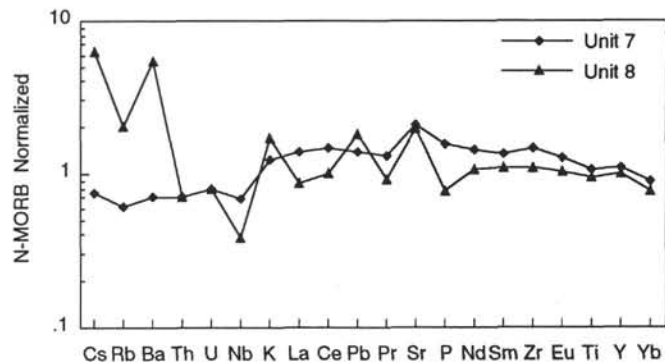


Figure 10. Comparison between the incompatible trace element contents of Units 7 and 8. The trace element data have been normalized to the N-MORB composition of Sun and McDonough (1989). Note the marked enrichments and decoupling between some elements in Unit 8, which are far in excess of what might be produced by a slightly higher degree of fractional crystallization modeled in these rocks (analyses from Table 5; Unit 7 represented by Section 135-834B-33R-1, 0–6 cm, and Unit 8 by Section 135-834B-36R-1, 0–7 cm).

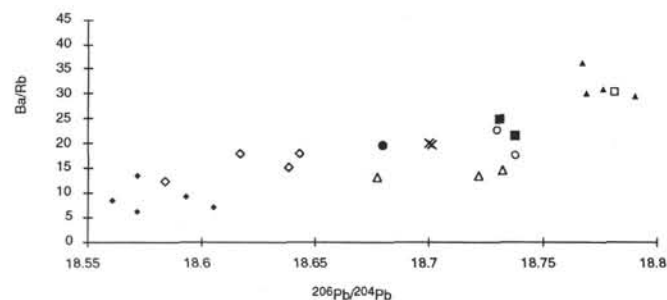


Figure 11. Ba/Rb vs. $^{206}\text{Pb}/^{204}\text{Pb}$ for Site 834 illustrating how the change in the incompatible element ratio is closely linked to the mixing process identified from the Pb-isotope variations. Symbols as in Figure 4.

sitions from 'Eua and Tafahi, the possible end-members suggested from the Pb-isotope data. The difference in Nb contents between Unit 7 (1.5 ppm) and Unit 8 (0.9 ppm) is approximately a factor of 2; therefore, the arc component must make up at least ~50% of the mixture that generated Unit 8. Less than a 50% contribution, and the "arc" end-member would be required to have a negative Nb content!

Assuming that Unit 8 represents a 50:50 mix of an arc component and a MORB component (Unit 7), we have calculated the trace element composition of the required model arc end-member (Fig. 12 and Table 6). Shown on Figure 12A are the few published data from 'Eua (Ewart and Bryan, 1972; Oversby and Ewart, 1972) and Tafahi (Pearce, unpubl. data). Figure 12B illustrates the same model composition compared with a representative from the Lau Volcanic Group (LVG = 14.0–5.4 Ma; Whelan et al., 1985; Woodhall, 1985) erupted on the island of Lakeba (refer to Fig. 1; Cole et al., 1985). Unfortunately, the suite of elements analyzed for the 'Eua and LVG samples is less extensive than that for Tafahi and the Site 834 lavas making comparison difficult. Tafahi has more pronounced depletions in Zr, Ti, and Y than our model arc composition and, as these elements cannot be matched by varying the degree of melting and/or fractionation, Tafahi magmas therefore cannot provide a suitable arc end-member for the Site 834 magmas. In contrast, the limited data from 'Eua provide a remarkably close match with the required "arc" end-member. Although the comparison between the Lakeba sample and the model arc composition is poor, it does show a broadly similar pattern with greatest mismatch between the more incompatible elements (i.e., more easily influenced by melting and fractionation processes).

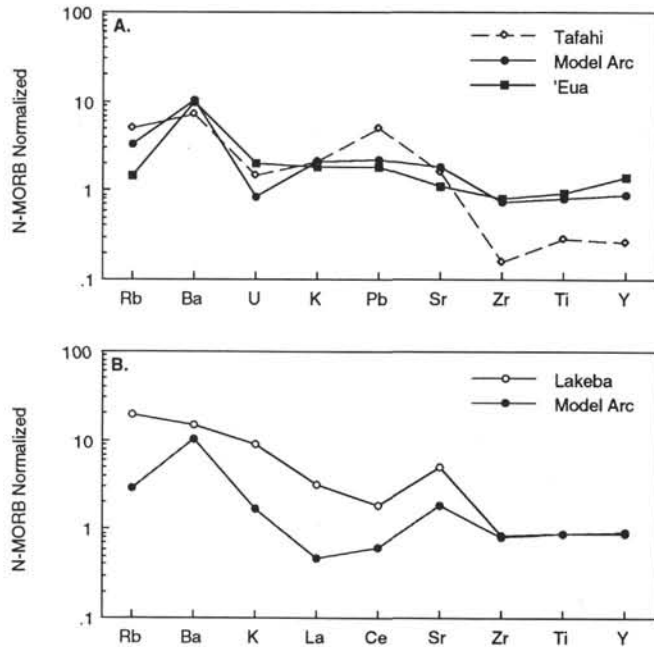


Figure 12. N-MORB normalized diagrams of the model arc composition (Table 6), with data from Tafahi, 'Eua, and Lakeba (LVG) shown for comparison. **A.** 'Eua shows a remarkably similar pattern, whereas the HFSEs and HREEs show significantly lower values in the Tafahi sample. **B.** Although discrepancy exists in the more incompatible elements toward the left of the diagram, the general shape of the Lakeba sample is similar to the required IAB end-member. Data are from Ewart and Bryan (1972), Pearce (unpubl. data), and Cole et al. (1985). Normalizing values are from Sun and McDonough (1989).

To test our hypothesis that the Unit 8 samples represent a 50:50 mix of N-MORB and a composition similar to volcanics from the original arc, we have calculated the isotopic ratios that would be predicted from the element concentrations and isotopic ratios of the end-members. Using the Pb data of Oversby and Ewart (1972) for 'Eua, we observe a very close match between predicted Pb-isotope ratios and those observed in Unit 8 (Table 6). Any increase in the proportion of the 'Eua end-member would result in Pb-isotopic compositions that are more radiogenic than any observed at Site 834. Despite the small amount of relevant data, we have attempted to make similar calculations for the other isotopic systems. Cole et al. (1990) plot a single data point in Sr-Nd space for 'Eua, quoting the source as McCulloch (unpubl. data). The Sr-isotope composition appears to be approximately 0.7032; using a 50:50 mixture of N-MORB and this 'Eua composition, the resultant $^{87}\text{Sr}/^{86}\text{Sr}$ composition for Unit 8 would be 0.7028, which is in remarkably close agreement with the measured ratios (0.702814). However, this mixture would predict a Sr concentration for the calculated mixture that is almost 20% lower than we observe. If the calculation is repeated to match the Sr content of Unit 8 rather than the isotopic ratio, the Sr-isotope ratio increases to only 0.7029, and, because plagioclase fractionation (or suppression) in either the end-member compositions or the observed Unit 8 composition can alter the Sr content, we consider the agreement is acceptable. In addition to the Pb-isotope compositions then, the Sr systematics also support the simplified model we present.

The $^{143}\text{Nd}/^{144}\text{Nd}$ composition of the 'Eua sample appears to be 0.51311, within the analytical uncertainty of all Site 834 rocks. As a result of their similarity in $^{143}\text{Nd}/^{144}\text{Nd}$ this composition provides no direct constraint on the mixing model being tested; however, it might explain how such large proportions of arc component can be accommodated in the Unit 8 mixtures without deviation from Nd-isotopic values observed in Unit 7.

Table 6. Calculated composition of the required model arc component.

	Unit 7 (average)	Unit 8 (average)	Model arc	'Eua	'Unit 8' calculated
Rb	0.6	1.1	1.6	0.8	0.7
Ba	5	35	65	61	33
U	0.042	0.035	0.028	0.096	0.069
K ₂ O	0.09	0.11	0.12	0.19	0.14
Pb	0.49	0.56	0.63	0.55	0.52
Sr	183	175	168	100	141
Zr	100	80	61	59	79
TiO ₂	1.35	1.24	1.12	1.17	1.26
Y	29	27	26	39	34
$^{206}\text{Pb}/^{204}\text{Pb}$	18.58	18.78		18.90	18.75
$^{207}\text{Pb}/^{204}\text{Pb}$	15.48	15.54		15.57	15.53
$^{208}\text{Pb}/^{204}\text{Pb}$	38.04	38.40		38.64	38.36
$^{87}\text{Sr}/^{86}\text{Sr}$	0.70254	0.70281		0.70320	0.70277
$^{143}\text{Nd}/^{144}\text{Nd}$	0.51311	0.51313		0.51311	

Notes: The calculation simply assumes that a 50:50 mixture between IAB and the average composition of Unit 7 will yield the Unit 8 magmas and so is derived by straightforward mass balance (i.e., $[\text{IAB} \times 0.5] + [\text{Unit 7} \times 0.5] = \text{Unit 8}$). Comparison between this calculated model arc and data for rocks from 'Eua can be made by contrasting the values in columns 3 and 4. To cross-check, we have used the actual data for 'Eua (unfortunately drawn together from different samples because of the poor amount of data available; data from Oversby and Ewart [1972], Ewart and Bryan [1972], and McCulloch [unpubl. data]) and recalculated a 50:50 mix of true arc and average Unit 7. The results are listed in column 5 and include the estimates of the Pb- and Sr-isotopic compositions for Unit 8. Clearly, some significant discrepancies are present between this "calculated Unit 8" and the measured values. In particular, Rb and Sr are quite high and U is rather low in the true composition, compared with the calculation based on 'Eua. Nonetheless, other elements are more closely matched, and the isotopic ratios are remarkably close. No calculation was made for Nd, mainly because of the complete overlap between isotopic compositions, but also because Nd elemental concentrations are lacking for the 'Eua samples used. Similar calculations can be made using the Lakeba sample (see text); however, this sample lacks key Pb-isotope data at present and is not included in this table (refer to Fig. 12B for the trace element comparison).

So far, this discussion has centered on the similarities of 'Eua to our model arc end-member because it is the only one of the original Tongan islands known to display suitable Pb-isotope compositions and trace element characteristics. The rocks from islands within the Lau Ridge may also provide suitable end-member compositions and have latitudes more adjacent to Site 834. Although the work is currently underway, at present, no Pb-isotope data are available for samples from the LVG that might be related to contemporaneous magmatism at Site 834. In some respects, samples from 'Eua, and members of the LVG are very similar. For example, Cole et al. (1990) illustrate a close similarity in the degree of source depletion between LVG rocks and samples from 'Eua based on $\text{Al}_2\text{O}_3/\text{TiO}_2$ vs. CaO/TiO_2 . (If additional data from Ewart and Bryan [1972] and Cunningham and Anscombe [1985] are added to this diagram, the overlap is complete.) The Sr- and Nd-isotope compositions for the LVG are also close to the single data point for 'Eua (Cole et al., 1990). As noted in Figure 12B, the trace element features of samples from Lakeba are also broadly similar to those required of the "arc" end-member, although none appear to have compositions as close to our model arc as 'Eua.

If the magmas from Unit 8 were generated by an approximately 50:50 mix of Pacific MORB and our model arc, the other units represent mixtures having between 10% (Unit 6) and 50% (Unit 2) of the arc end-member. Results of this simple model have been overlain on the plot of Ba/Rb vs. $^{206}\text{Pb}/^{204}\text{Pb}$ to illustrate the magnitude of deviations between the calculated and observed data (Fig. 13A). Unfortunately, because most units have undergone significant fractional crystallization and the concentrations of various elements have been thereby modified, other comparisons are fraught with difficulties. The type of simple calculations we propose might broadly explain the unusual offsets observed in some "element vs. MgO" diagrams (Fig.

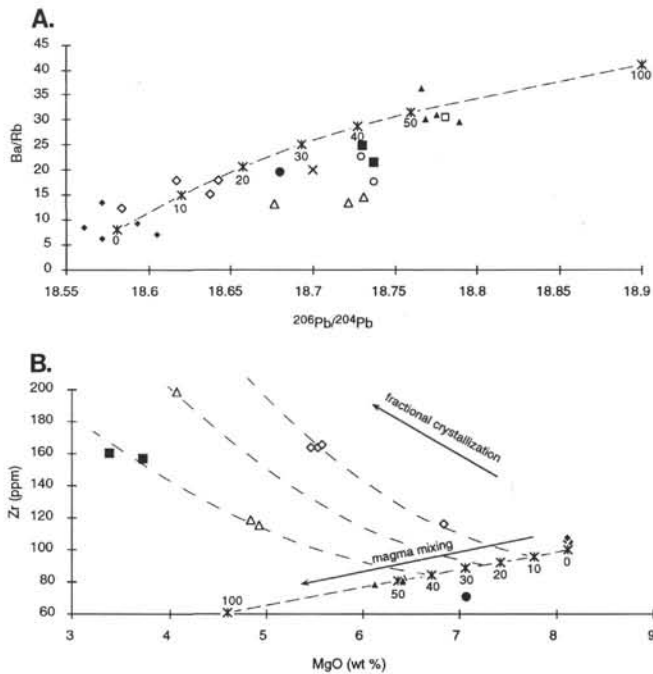


Figure 13. Two of the plots presented earlier (from Figs. 5 and 11), modified to show where the modeled arc–Unit 7 mixtures plot relative to the real data. **A.** In the case of Ba/Rb, this ratio is unaffected by subsequent fractional crystallization, and the comparison is very encouraging. **B.** In contrast, the Zr and MgO contents are strongly modified during crystal fractionation, and the diagram presented here attempts to illustrate how the mixing model might explain the apparent scatter observed in the plots of HFSEs and REEs vs. MgO content illustrated in Figure 5. Percentage labels are given for 0% IAB contributions (i.e., pristine MORB) up to 100%, or pure IAB. Note that this may also explain some of the mismatch in major element compositions with the model shown in Figure 9 (e.g., Na_2O and TiO_2) because of the fractionation from different parental compositions.

13B). Although we do not wish to imply that mixing must occur between magmas with exactly the same major element compositions as Unit 7 and our model arc, Figure 13B shows how a range of mixtures may differentiate to produce a spectrum of subparallel fractionation curves that might otherwise be ignored as scatter.

Timing

Constraining the timing of mixing relative to melt generation and fractional crystallization can reveal information regarding the proximity of the end-members and the dynamics of magmatism. As previously described, most of the major element variations of the Site 834 samples are generally consistent with low-pressure fractional crystallization of a MORB-like parent composition. Although we cannot obtain many constraints on the timing of the mixing processes from the major element compositions, we can eliminate two possibilities.

If these samples were simply related by fractional crystallization, we would expect homogeneous isotopic compositions among the samples, and this is patently not the case. In addition, the kinked major element profiles reflect fractional crystallization rather than mixing and no correlation exists between isotopic and major element compositions, so the signatures cannot reflect assimilation that occurred during fractionation of a single magma batch. Thus, we can only conclude that the major element variations generally reflect very similar crystallization processes operating on magmas with broadly similar mineralogies. The implication is that mixing must have taken place before significant magma differentiation. The repetition of key

signatures (e.g., $^{206}\text{Pb}/^{204}\text{Pb}$) with depth further indicates that mixing events were repeated throughout the petrogenetic history of the Site 834 lavas.

Mixing could reflect (1) interaction of two primitive magmas, (2) variable partial melting and mixing of an upwelling “two-component” source region, or (3) the assimilation of IAB lithosphere by an upwelling N-MORB magma. In truth, there is no foolproof method of distinguishing between these possibilities. We can say, however, that if assimilation of lithospheric material (e.g., old Eua-like basement) occurred, then certain aspects of the N-MORB end-member need to be modified. If the MORB magma is required to crystallize to provide the heat necessary for a maximum of ~50% wholesale crustal assimilation, its starting composition must have been far more magnesian than that of Unit 7. Although possible, this may be unlikely given that Unit 7 already has an MgO content (>8 wt%) greater than most erupted N-MORB that have not assimilated crust, and an Mg# of around 65 that would drop rapidly during significant fractional crystallization. An alternative is that previously emplaced melts could cool, crystallize, and provide the heat required to melt the lithosphere with subsequent magmas coming through and mixing with this melted crust. We consider this unlikely because the “contaminant” magma would then be of granitic composition rather than the mafic end-member low in many incompatible trace elements that we think is required to generate mafic, yet heavily contaminated N-MORB magmas, such as Unit 8. The results of the simple mass-balance calculations (Figs. 12–13 and Table 6), coupled with the fractionation signature of the major elements (Fig. 2), are encouraging and support a case for magma mixing between two relatively mafic end-members. Such mixing processes satisfactorily explain both the range in trace element characteristics and the isotopic compositions of basalts from Site 834.

Progressive partial melting of an upwelling two-component source region (i.e., N-MORB and IAB) is impossible to refute; however, this becomes something of a semantic argument. It is possible that a mixed source upwells beneath the region of extension and gives rise to one type of melt (IAB?), which then progressively gives way to more MORB-like compositions until the next “package” of mantle material is introduced into the zone of melting. What is difficult to reconcile with this model is the presence of pure N-MORB material given that there is likely to be at least some of the IAB component around at all times.

We note that IAB was being produced in the ancient arc and did not cease with the initiation of extension and development of the Lau Basin (as evidenced from the sedimentary records and new minimum age for the basement at Site 834; see Parson, Hawkins, Allan, et al., 1992). Given that (1) IAB was available at the time, (2) pure N-MORB is present in the drilled section, and (3) simple mixing calculations are successful in generating the Unit 8 basalts, we propose that the most likely mechanism for generating the lavas at Site 834 is one of magma mixing between relatively mafic mantle end-members early in the petrogenesis of these rocks. This process dominates the ratios between some trace elements and explains the isotopic compositions, whereas subsequent fractional crystallization of the various mixtures gives rise to the trends that covary with indices of fractionation.

Dynamics

Magma mixing requires that both end-members are simultaneously available; in the suite of basalts recovered from Site 834, such a co-existence of sources is supported by progressive downhole variations and repetition of compositions (particularly evident in the Pb isotopes). As both MORB and arc-like end-members must be present during petrogenesis of the Site 834 lavas, there cannot be a continual progression away from IAB signatures with backarc basin evolution. The range of compositions preserved in this sequence of lavas is used to infer the dynamics of magmagenesis in the early extensional environment.

In their recent article concerning magmatism at mid-ocean spreading centers, Sinton and Detrick (1992) propose a model describing

how the products of magmatism relate to the rates of spreading and magma supply. Although the extension at Site 834 may not be directly applicable to that associated with true seafloor spreading, it approximates the amagmatic development of graben structures found at very slowly spreading axes where the magma supply rate is low.

For slow spreading, Sinton and Detrick (1992) envisage a dike-like mush of partially crystallized magma beneath the rift, surrounded by a highly crystalline and rigid transition zone. Isolated pockets of magma in the transition zone may impart a porosity of 20%–40% and may allow melts to interact and migrate throughout the matrix. The low magma supply rate in slow spreading centers causes eruptions to be closely coupled with new injections of melt from the underlying mantle. Owing to the absence of continually replenished, rapidly convecting melt lenses (as is proposed for the fast spreading, high magma supply ridges), the magmas produced at slowly extending rifts do not reside in any traditional form of magma chamber and, when erupted, will be heterogeneous.

Although Sinton and Detrick (1992) developed their model using geophysical and geochemical observations from mid-ocean ridges, some aspects appear to match the chemistry of the melts produced at Site 834 during extension and rupture of the Tongan arc. One important difference is that IAB volcanism was occurring in the arc at the time of extension and upwelling asthenospheric mantle was destined to interact with melts located in the sub-arc wedge. The cartoon sketched in Figure 14 illustrates our modification of the slow-spreading, low magma supply rate case of Sinton and Detrick (1992). The repetition of compositions at Site 834 is consistent with eruptions that are triggered by new injections of asthenospheric magma. We envisage that the initial pulse will combine with relatively large proportions of arc melt in the wedge to produce mixtures similar to those observed in Unit 8. Because this removes much of the available arc component, the very next melts extracted are those that most closely resemble N-MORB (i.e., Unit 7). In their wake, various mixtures of the two end-members form as melt migration of both end-members into the zone of magmatism occurs, and these may stall and fractionate in isolated melt pockets before being erupted (e.g., Subunit 10a and Unit 12). As the supply of upwelling MORB is shut off, migration of arc melts into the mush zone continues unhampered, awaiting the next pulse of MORB magma.

It is interesting to note that the depth over which the N-MORB Unit 7 was recovered is greater than that for any of the other units from Site 834. Although there is no strong correlation between the apparent thickness of the units and the degree of mixing with the IAB end-member, the most highly contaminated MORB melts (i.e., Units 2 and 8) are amongst thinnest of the 13 units recovered. We propose that the volume of N-MORB involved in the magmatic cycles is greater than the amount of IAB available explaining both why no pure IAB is erupted, and why the MORB end-member dominates the products observed. The repetition of compositions as observed is similar to that expected from magmatism triggered by the periodic injection of fresh MORB melt, and the compositional range of products argues against the existence of an homogenizing magma chamber.

CONCLUSIONS

The magmas erupted during the initial stages of backarc rifting represent a variety of mixtures between Pacific MORB and arc end-member magmas. The arc component was similar in composition to rocks on 'Eua, or Lakeba (LVG) from the "old" Tongan arc, and the Pacific end-member indicates that the mantle underlying the original arc was derived from the Pacific mantle convection cell. The latter observation has implications for the mantle dynamics in the region, as ML basalts show closer affinities with MORB from the Indian Ocean. It is not clear how Pacific style mantle became trapped to the west of the subducting plate (an ancient trench jump, or subduction reversal perhaps?); however, the clear implication is that the Pacific

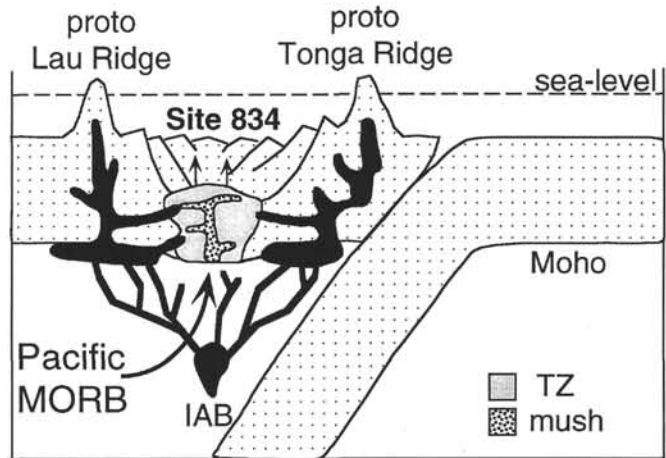


Figure 14. Cartoon modified from Sinton and Detrick (1992) based on their description of magmatism at slow-spreading, low-magma-supply extensional regimes. Their model is based on ocean-ridge data; however, some of their observations might also apply to the initial stages of opening of the Lau Basin. The black regions seek to illustrate IAB that continues to erupt within the slowly fragmenting arc (e.g., LVG), but is also either drawn into the source of extension-related magmas, and/or variably contaminates MORB melts as they pass through the wedge. TZ signifies the outer region surrounding the mush zone and has been termed the "transition zone" by Sinton and Detrick (1992). An arrow shows an influx of "fresh" Pacific N-MORB, some of which must penetrate the wedge without significant modification (e.g., Unit 7). We propose that this influx is only likely if significant rollback of the descending slab occurs.

material has been replaced by an Indian Ocean-like MORB source during the last ~5.5 Ma.

Results from simple mass-balance calculations using the most and least radiogenic compositions from Site 834 suggest that the range of compositions extend from essentially pristine MORB (Unit 7) to mixtures in which up to 50% of the end product is derived from the arc end-member (Units 2 and 8).

Magma mixing occurred before most of the fractional crystallization now preserved in the rocks from Site 834. Major element trends are consistent with fractionation (at approximately 1 kb) of a MORB-like parent, in which plagioclase crystallization has been suppressed owing to relatively high H₂O contents.

Evidence for magma mixing, coupled with the downhole repetition of many chemical features, indicates that both MORB and IAB components were simultaneously available, and that magmatism was probably triggered by fresh injections of MORB material. As an important corollary to this, compositions did not systematically change from arc-like to MORB-like with time. Even in the very earliest stages of backarc extension, pristine N-MORB material was being delivered to the mantle wedge and erupted.

The mechanism for arc rupture most consistent with the observed geochemistry, is one of slow and almost amagmatic extension similar to that recently described by Sinton and Detrick (1992). This is also consistent with the horst-and-graben topography of the western Lau Basin.

Clearly, arc magmatism does not immediately cease with the onset of extension and rifting. Volcanism continued in the Lau Ridge and at 'Eua (still adjacent at that time) while an enormous spectrum of compositions were erupting in a nearby graben structure (the location of Site 834). Not surprisingly, many of Site 834 basalts show geochemical affinities to IABs; however, the range of basalts also includes MORB compositions closer to typical N-MORB than the modern Lau Basin lavas erupting at well-developed spreading centers (see also Hergt and Hawkesworth, this volume).

The fact that fertile N-MORB mantle was available during the earliest stages of backarc extension implies that an influx of this

material accompanied the change in tectonic regime. To accommodate (or, indeed, initiate) an influx of fresh asthenosphere, we propose that significant rollback of the slab must have occurred.

ACKNOWLEDGMENTS

We would very much like to thank our friends and colleagues who sailed on Leg 135. Special thanks to the crew for their skill, patience, and friendship; thanks also to the science party in general for being great fun. We extend special gratitude to our fellow igneous petrologists, both for handing over all of that glass, and for their support both on and since the cruise; we owe you guys!! We would also like to take this opportunity to thank Sarah Roeske for her help in generating the probe data, Terry Plank for assistance with the LLD calculations, and Mabs Johnston and Peter van Calsteren in maintaining the excellent lab and machine facilities necessary for conducting the isotope work. JMH would also like to thank Julian Pearce and Dave Peate for their help in generating the ICP-MS results, and Allen Kennedy for helping to put final touches to the manuscript! Others include Ken Farley, Chris Hawkesworth, Bill McDonough, Steve Eggins, Ted Ringwood, and Shen-su Sun for their careful and helpful suggestions on previous drafts of this manuscript; and, of course, Bob Stern and Rebecca Lange for their detailed and critical reviews. Financial support for the probe analyses was provided by USSAC to KN, and JMH gratefully acknowledges both financial and moral support from NERC; thanks Lin!

REFERENCES*

- Bender, J.F., Langmuir, C.H., and Hanson, G.N., 1984. Petrogenesis of basalt glasses from the Tamayo region, East Pacific Rise. *J. Petrol.*, 25:213–254.
- Ben Othman, D., White, W.M., and Patchett, J., 1989. The geochemistry of marine sediments, island arc magma genesis and crust-mantle recycling. *Earth Planet. Sci. Lett.*, 94:1–21.
- Bryan, W.B., 1986. Linked evolutionary data arrays: a logical structure for petrologic modeling of multisource, multiprocess magmatic systems. *J. Geophys. Res.*, 91:5881–5900.
- Byerly, G.R., Melson, W.G., and Vogt, P.R., 1976. Rhyodacites, andesites, ferro-basalts and ocean tholeiites from the Galapagos Spreading Center. *Earth Planet. Sci. Lett.*, 30:215–221.
- Byers, C.D., Muenow, D.W., and Garcia, M.O., 1983. Volatiles in basalts and andesites from the Galapagos Spreading Center, 85 to 86°W. *Geochim. Cosmochim. Acta*, 47:1551–1558.
- Christie, D.M., and Sinton, J.M., 1986. Major element constraints on melting, differentiation and mixing of magmas from the Galapagos 95.5°W propagating rift system. *Contrib. Mineral. Petrol.*, 94:274–288.
- Cole, J.W., Gill, J.B., and Woodhall, D., 1985. Petrologic history of the Lau Ridge, Fiji. In Scholl, D.W., and Vallier, T.L. (Eds.), *Geology and Offshore Resources of Pacific Island Arcs—Tonga Region*. Circum-Pac. Coun. Energy Miner. Resour., Earth Sci. Ser., 2:379–414.
- Cole, J.W., Graham, I.J., and Gibson, I.L., 1990. Magmatic evolution of Late Cenozoic volcanic rocks of the Lau Ridge, Fiji. *Contrib. Mineral. Petrol.*, 104:540–554.
- Cunningham, J.K., and Anscombe, K.J., 1985. Geology of 'Eua and other islands, Kingdom of Tonga. In Scholl, D., and Vallier, T. (Eds.), *Geology and Offshore Resources of Pacific Island Arcs—Tonga Region*. Circum-Pac. Coun. Energy Miner. Resour., Earth Sci. Ser., 2:221–258.
- Drake, M.J., 1976. Plagioclase-melt equilibria. *Geochim. Cosmochim. Acta*, 40:457–465.
- Ernewein, M., Pearce, J.A., Bloomer, S.H., Parson, L.M., Murton, B.J., and Johnson, L.E., in press. Geochemistry of Lau Basin volcanic rocks: influence of ridge segmentation and arc proximity. In Smellie, J. (Ed.), *Volcanism Associated with Extension at Consuming Plate Margins*. Geol. Soc. Spec. Publ. London.
- Ewart, A., and Bryan, W., 1972. Petrography and geochemistry of the igneous rocks from 'Eua, Tonga Islands. *Geol. Soc. Am. Bull.*, 83:3281–3298.
- Ewart, A., and Hawkesworth, C.J., 1987. The Pleistocene-Recent Tonga-Kermadec arc lavas: interpretation of new isotope and rare earth data in terms of a depleted mantle source model. *J. Petrol.*, 28:495–530.
- Fryer, P., Taylor, B., Langmuir, C.H., and Hochstaedter, A.G., 1990. Petrology and geochemistry of lavas from the Sumisu and Torishima backarc rifts. *Earth Planet. Sci. Lett.*, 100:161–178.
- Furlong, K.P., Chapman, D.S., and Alfeld, P.W., 1982. Thermal modelling of the geometry of subduction with implications for the tectonics of the overlying plate. *J. Geophys. Res.*, 87:1756–1802.
- Garfunkel, Z., Anderson, C.A., and Schubert, G., 1986. Mantle circulation and the lateral migration of subducted slabs. *J. Geophys. Res.*, 91:7205–7223.
- Gill, J.B., 1976. Composition and age of Lau basin and ridge volcanic rocks: implications for evolution of an interarc basin and remnant arc. *Geol. Soc. Am. Bull.*, 87:1384–1395.
- Hawkins, J.W., Bloomer, S.H., Evans, C.A., and Melchior, J.T., 1984. Evolution of intra-oceanic arc-trench systems. *Tectonophysics*, 102:175–205.
- Hawkins, J.W., Lonsdale, P.F., Macdougall, J.D., and Volpe, A.M., 1990. Petrology of the axial ridge of the Mariana Trough backarc spreading center. *Earth Planet. Sci. Lett.*, 100:226–256.
- Hawkins, J.W., and Melchior, J.T., 1985. Petrology of Mariana Trough and Lau Basin basalts. *J. Geophys. Res.*, 90:11431–11468.
- Helz, R.T., 1976. Phase relations of basalts in their melting ranges at $PH_2O = 5$ kb. Part II. Melt compositions. *J. Petrol.*, 17:139–193.
- Hochstaedter, A.G., Gill, J.B., Kusakabe, M., Newman, S., Pringle, M., Taylor, B., and Fryer, P., 1990. Volcanism in the Sumisu Rift. I. Major element, volatile and stable isotope geochemistry. *Earth Planet. Sci. Lett.*, 100:179–194.
- Hofmann, A.W., Jochum, K.P., Seufert, M., and White, W.M., 1986. Nb and Pb in oceanic basalts: new constraints on mantle evolution. *Earth Planet. Sci. Lett.*, 79:33–45.
- Hynes, A., and Mott, J., 1985. On the causes of backarc spreading. *Geology*, 13:387–389.
- Jarrard, R.D., 1986. Relations among subduction parameters. *Rev. Geophys.*, 24:217–284.
- Jenner, G.A., Cawood, P.A., Rautenschlein, M., and White, W.M., 1987. Composition of backarc basin volcanics, Valu Fa Ridge, Lau Basin: evidence for a slab-derived component in their mantle source. *J. Volcanol. Geotherm. Res.*, 32:209–222.
- Karig, D.E., 1970. Ridges and basins of the Tonga-Kermadec island arc system. *J. Geophys. Res.*, 75:239–254.
- Langmuir, C.H., Zhang, Y., Taylor, B., Plank, T., and Rubenstone, J., in press. Petrogenesis of Torishima and adjacent volcanos of the Izu-Bonin Arc: one end-member of the global spectrum of arc basalt compositions. *Contrib. Mineral. Petrol.*
- Lawver, L., and Hawkins, J.W., 1978. Diffuse magnetic anomalies in marginal basins: their possible petrologic and tectonic significance. *Tectonophysics*, 43:323–339.
- le Roex, A.P., Dick, H.J.B., Reid, A.M., Frey, F.A., Erlank, A.J., and Hart, S.R., 1985. Petrology and geochemistry of basalts from the American-Antarctic Ridge, Southern Ocean: implications for the westward influence of the Bouvet mantle plume. *Contrib. Mineral. Petrol.*, 90:367–380.
- Loock, G., McDonough, W.F., Goldstein, S.L., and Hofmann, A.W., 1990. Isotopic compositions of volcanic glasses from the Lau Basin. *Mar. Min.*, 9:235–245.
- Nielsen, R.L., 1988. A model for the simulation of combined major and trace element liquid lines of descent. *Geochim. Cosmochim. Acta*, 52:27–38.
- Oversby, V.M., and Ewart, A., 1972. Lead isotopic compositions of Tonga-Kermadec volcanics and their petrogenetic significance. *Contrib. Mineral. Petrol.*, 37:181–210.
- Parson, L., Hawkins, J., Allan, J., et al., 1992. *Proc. ODP, Init. Repts.*, 135: College Station, TX (Ocean Drilling Program).
- Parson, L.M., Hawkins, J.W., and Hunter, P.M., 1992. Morphotectonics of the Lau Basin seafloor—implications for the opening history of backarc basins. In Parson, L., Hawkins, J., Allan, J., et al., *Proc. ODP, Init. Repts.*, 135: College Station, TX (Ocean Drilling Program), 81–82.
- Parson, L.M., Pearce, J.A., Murton, B.J., Hodkinson, R.A., Bloomer, S., Ernewein, M., Huggett, Q.J., Miller, S., Johnson, L., Rodda, P., and Helu, S., 1990. Role of ridge jumps and ridge propagation in the tectonic evolution of the Lau backarc basin, southwest Pacific. *Geology*, 18:470–473.
- Schilling, J.-G., Zajac, M., Evans, R., Johnson, T., White, W., Devine, J.D., and Kingsley, R., 1983. Petrologic and geochemical variations along the Mid-Atlantic Ridge from 29°N to 75°N. *Am. J. Sci.*, 283:510–586.
- Sinton, J.M. and Detrick, R.S., 1992. Mid-ocean ridge magma chambers. *J. Geophys. Res.*, 97:197–216.

* Abbreviations for names of organizations and publication titles in ODP reference lists follow the style given in *Chemical Abstracts Service Source Index* (published by American Chemical Society).

- Sinton, J.M., and Fryer, P., 1987. Mariana Trough lavas from 18°N: implications for the origin of backarc basin basalts. *J. Geophys. Res.*, 92:12782–12802.
- Spulber, S.D., and Rutherford, M.J., 1983. The origin of rhyolite and plagiogranite in oceanic crust: an experimental study. *J. Petrol.*, 24:1–25.
- Stern, R.J., Lin, P.-N., Morris, J.D., Jackson, M.C., Fryer, P., Bloomer, S.H., and Ito, E., 1990. Enriched back-arc basin basalts from the northern Mariana Trough: implications for the magmatic evolution of back-arc basins. *Earth Planet. Sci. Lett.*, 100:210–225.
- Sun, S.-S., and McDonough, W.F., 1989. Chemical and isotopic systematics of oceanic basalts: implications for mantle composition and processes. In Saunders, A.D., and Norry, M.J. (Eds.), *Magmatism in the Ocean Basins*. Geol. Soc. Spec. Publ. London, 42:313–345.
- Sunkel, G., 1990. Origin of petrological and geochemical variations of Lau Basin lavas (SW Pacific). *Mar. Min.*, 9:205–234.
- Tarney, J., Saunders, A.D., Matthey, D.P., Wood, D.A., and Marsh, N.G., 1981. Geochemical aspects of backarc spreading in the Scotia Sea and western Pacific. *Philos. Trans. R. Soc. London A*, 300:263–285.
- Taylor, B., and Karner, G.D., 1983. On the evolution of marginal basins. *Rev. Geophys. Space Phys.*, 21:1727–1741.
- Volpe, A.M., Macdougall, J.D., and Hawkins, J.W., 1988. Lau Basin basalts (LBB): trace element and Sr-Nd isotopic evidence for heterogeneity in backarc basin mantle. *Earth Planet. Sci. Lett.*, 90:174–186.
- Weaver, J.S., and Langmuir, C.H., 1990. Calculation of phase equilibrium in mineral-melt systems. *Computers Geosci.*, 16:1–19.
- Whelan, P.M., Gill, J.B., Kollman, E., Duncan, R., and Drake, R.E., 1985. Radiometric dating of magmatic stages in Fiji. In Scholl, D., and Vallier, T. (Eds.), *Geology and Offshore Resources of Pacific Island Arcs—Tonga Region*. Circum-Pac. Counc. Energy Miner. Resour., Earth Sci. Ser., 2:415–440.
- Woodhall, D., 1985. Geology of the Lau Ridge. In Scholl, D., and Vallier, T.L. (Eds.), *Geology and Offshore Resources of Pacific Island Arcs—Tonga Region*. Circum-Pac. Counc. Energy Miner. Resour., Earth Sci. Ser., 2:351–378.

Date of initial receipt: 29 June 1992

Date of acceptance: 5 May 1993

Ms 135SR-144